



**HAL**  
open science

## Turbidite-induced re-oxygenation episodes of the sediment-water interface in a diverticulum of the Tethys Ocean during the Oceanic Anoxic Event 1a: The French Vocontian Basin

Alexis Caillaud, Melesio Quijada, Bastien Huet, Jean-yves Reynaud, Armelle Riboulleau, Viviane Bout-roumazeilles, François Baudin, Anthony Anthony Chappaz, Thierry Adatte, Jean-noël Ferry, et al.

► **To cite this version:**

Alexis Caillaud, Melesio Quijada, Bastien Huet, Jean-yves Reynaud, Armelle Riboulleau, et al.. Turbidite-induced re-oxygenation episodes of the sediment-water interface in a diverticulum of the Tethys Ocean during the Oceanic Anoxic Event 1a: The French Vocontian Basin. *Depositional Record*, 2020, 6, pp.352 - 382. 10.1002/dep2.102 . hal-02862330v1

**HAL Id: hal-02862330**

**<https://hal.science/hal-02862330v1>**

Submitted on 16 Apr 2021 (v1), last revised 9 Jun 2020 (v2)

**HAL** is a multi-disciplinary open access archive for the deposit and dissemination of scientific research documents, whether they are published or not. The documents may come from teaching and research institutions in France or abroad, or from public or private research centers.

L'archive ouverte pluridisciplinaire **HAL**, est destinée au dépôt et à la diffusion de documents scientifiques de niveau recherche, publiés ou non, émanant des établissements d'enseignement et de recherche français ou étrangers, des laboratoires publics ou privés.



Distributed under a Creative Commons Attribution - NoDerivatives 4.0 International License

# Turbidite-induced re-oxygenation episodes of the sediment-water interface in a diverticulum of the Tethys Ocean during the Oceanic Anoxic Event 1a: The French Vocontian Basin

Alexis Caillaud<sup>1</sup> | Melesio Quijada<sup>1</sup> | Bastien Huet<sup>1</sup> | Jean-Yves Reynaud<sup>1</sup> |  
 Armelle Riboulleau<sup>1</sup> | Viviane Bout-Roumazelles<sup>1</sup> | François Baudin<sup>2</sup> |  
 Anthony Chappaz<sup>3</sup> | Thierry Adatte<sup>4</sup> | Jean-Noël Ferry<sup>5</sup> | Nicolas Tribovillard<sup>1</sup> 

<sup>1</sup>Laboratoire d'Océanologie et de Géosciences, UMR 8187 LOG CNRS, Université de Lille-ULCO, Wimereux, France

<sup>2</sup>Sorbonne Université, UPMC Univ, CNRS, ISTEP, Paris, France

<sup>3</sup>Department of Earth and Atmospheric Sciences, Central Michigan University, Mount Pleasant, MI, USA

<sup>4</sup>Institute of Earth Sciences, University of Lausanne, Lausanne, Switzerland

<sup>5</sup>TOTAL S.A, CSTJF, Pau, France

## Correspondence

Nicolas Tribovillard, Laboratoire d'Océanologie et de Géosciences, UMR 8187 LOG CNRS-Université de Lille-ULCO, Wimereux, France.  
 Email: nicolas.tribovillard@univ-lille.fr

## Funding information

TOTAL S.A.

## Abstract

Widespread anoxic events affected the Tethys Ocean during the Mesozoic. The Ocean Anoxic Event 1a (Early Aptian), expressed as the Selli Level or Goguel Level (GL) in European basins. The GL was deposited in the French Vocontian Basin, a semi-enclosed basin connected to the Tethys Ocean. This study presents an integrated approach (Rock Eval, clay minerals, grain-size, inorganic geochemistry and molecular biomarkers), applied to four sections in the basin distributed along a proximal-distal transect. This study shows that the GL was perturbed by turbidites. In particular, the results demonstrate: (a) a homogeneous redox status of the basin that experienced oxic to suboxic conditions, according to trace element distributions and (b) low organic matter contents (total organic carbon *ca* 1 wt%) in the three sections where turbiditic deposits are observed. The distal, condensed section exhibits the highest organic matter contents (total organic carbon >3 wt%). In addition, the presence of gammacerane and isorenieratene derivatives in the distal sections suggests that the water-column was intermittently stratified, with hypoxia developing in the photic zone. This stratification did not result from strong surface productivity but more likely from: (a) limited renewal of deep water in the basin; (b) reputedly high surface-water palaeotemperatures during the Early Aptian; and (c) the influx of waters, possibly depleted in free oxygen and in some dissolved trace elements, into the basin. The turbiditic inputs, in addition to organic matter dilution in the sediments and a brief rupture of the water-column stratification in the proximal areas of the basin, ventilated the sea floor and more specifically re-oxidized the sediment-water interface as well as underlying sediments. Such episodes of benthic re-oxygenation could have altered the long-term palaeoredox record, even in the distal sections where reducing conditions prevailed during deposition. In the area deprived of turbiditic input, sedimentary condensation, coupled with low oxygen conditions, furthered organic matter preservation and concentration.

This is an open access article under the terms of the Creative Commons Attribution License, which permits use, distribution and reproduction in any medium, provided the original work is properly cited.

© 2020 The Authors. *The Depositional Record* published by John Wiley & Sons Ltd on behalf of International Association of Sedimentologists.

**KEYWORDS**

Clay minerals, Early Aptian, geochemistry, grain size, organic matter dilution, organic matter, palaeo-redox proxies, turbidites

## 1 | INTRODUCTION

The Tethys Ocean was affected by widespread anoxia as demonstrated by the presence of organic carbon enriched horizons found world-wide (Schlanger and Jenkyns, 1976; Jenkyns, 2010). These Oceanic Anoxic Events (OAEs) were catastrophic environmental issues because the absence of oxygen profoundly disturbed the whole marine ecosystem biota leading to mass extinctions. Nowadays, coastal areas are impacted by hypoxia (dead zones) and global OAEs might threaten our modern oceans as a consequence of climate changes and anthropogenic pressures on natural biogeochemical cycles (Baudin *et al.*, 2017 and references therein). Although the sedimentary records of OAEs have been extensively studied over the past 40 years (Arthur and Schlanger, 1979; Summerhayes, 1981; Jacquin and Graciansky, 1988; Br  h  ret, 1994; Leckie *et al.*, 2002; Jenkyns, 2003; Emeis and Weissert, 2009), the controls governing OAE dynamics commonly taken into consideration remain simplistic, and involve only the usual parameters (i.e. the levels of organic productivity and oxygenation conditions) to characterize ancient redox conditions prevailing during OAEs. In this paper, the focus is placed on the OAE 1a event that unfolded during the early Aptian. The corresponding deposits have been termed Niveau Goguel, or Goguel Level (GL), in the Vocontian Basin of south-eastern France (Br  h  ret, 1997), and Livello Selli, or Selli Level, in the Marche-Umbria Basin of Italy (Coccioni *et al.*, 1987). The Vocontian Basin is an ideal site for examining OAEs throughout the Mesozoic as it experienced a long-lasting phase of pelagic and hemipelagic sedimentation—markedly tuned to orbital Milankovitch-type cyclicities—with low depositional energy, allowing subtle environmental variations to be recorded (Br  h  ret, 1994; 1997). Recent investigations comparing the GL to its lateral equivalents in other settings or locations in the Tethys Ocean, such as Switzerland and Italy, were grounded on one or two sections only in the Vocontian Basin. Currently, integrated studies of the GL are still lacking, in particular concerning its distribution and heterogeneity in the Vocontian Basin. Here, several contrasted records of the GL are examined, particularly where it is frequently reworked or interbedded with turbidite deposits. The aim of the study is to assess the role of turbiditic activity in the enrichment and preservation of organic matter (OM). For this purpose, the GL was explored through four sections in the Vocontian Basin, using a multi-proxy approach: the organic geochemistry is used to determine the abundance and

nature of OM, and, in addition to field observations, the inorganic geochemistry, grain-size of the non-carbonate fraction and clay-mineral assemblage identification allow the depositional conditions prevailing during the OAE 1a in this diverticulum of the Tethys Ocean to be defined.

## 2 | GEOLOGICAL SETTING OF THE VOCONTIAN BASIN DURING THE APTIAN

During the Lower Cretaceous, the Vocontian Basin of south-eastern France corresponded to the slope of the northern margin of the Tethys Ocean (Fri  s and Parize, 2003, Figure 1). The platforms surrounding the basin were located in Provence to the south, Ard  che to the west, and the Chartreuse and Vercors mountains to the north (Figure 1). Thus, the Vocontian Basin was a diverticulum of the Tethys Ocean, only connected to the open ocean at its eastern end. The geometry of the Vocontian Basin was controlled by a system of extensive faults and tilted blocks inherited from Tethyan rifting, which occurred during Jurassic times (Graciansky and Lemoine, 1988). However, the Aptian and Albian stages were marked by a transition to an extensive–transpressive coupled tectonic system in the basin (Beaudoin *et al.*, 1986; Fri  s, 1987; Graciansky and Lemoine, 1988; Joseph *et al.*, 1989). The extensive tectonics may have been a consequence of the North Atlantic rifting (Graciansky and Lemoine, 1988), but the transpressive component indicates a more probable influence from the opening of the Bay of Biscay (Souquet, 1978; Ricou and Frizon de Lamotte, 1986; Joseph *et al.*, 1989; Hibschi *et al.*, 1992), as a consequence of anti-clockwise rotation of the Iberian Plate (Ziegler, 1990; Stampfli *et al.*, 1998). The basin morphology and sedimentation patterns were controlled by the tilted blocks (Fri  s and Parize, 2003). This structural control resulted in very different thicknesses of sediments being deposited at different locations in the Vocontian Basin. At the Aptian–Albian transition, the Provence Platform was uplifted, which resulted in the emersion of the so-called Durancian Isthmus (Gignoux, 1925; Rubino, 1989; Hibschi *et al.*, 1992; Masse *et al.*, 2000). On a larger scale, the first signs of compression have been dated as Cenomanian, based on the presence of a significant unconformity in the Vocontian Basin (Fri  s, 1987; Hibschi *et al.*, 1992), although a recent study has proposed that the closure of the Vocontian Basin could have started during the so-called ‘Austrian Event’ in

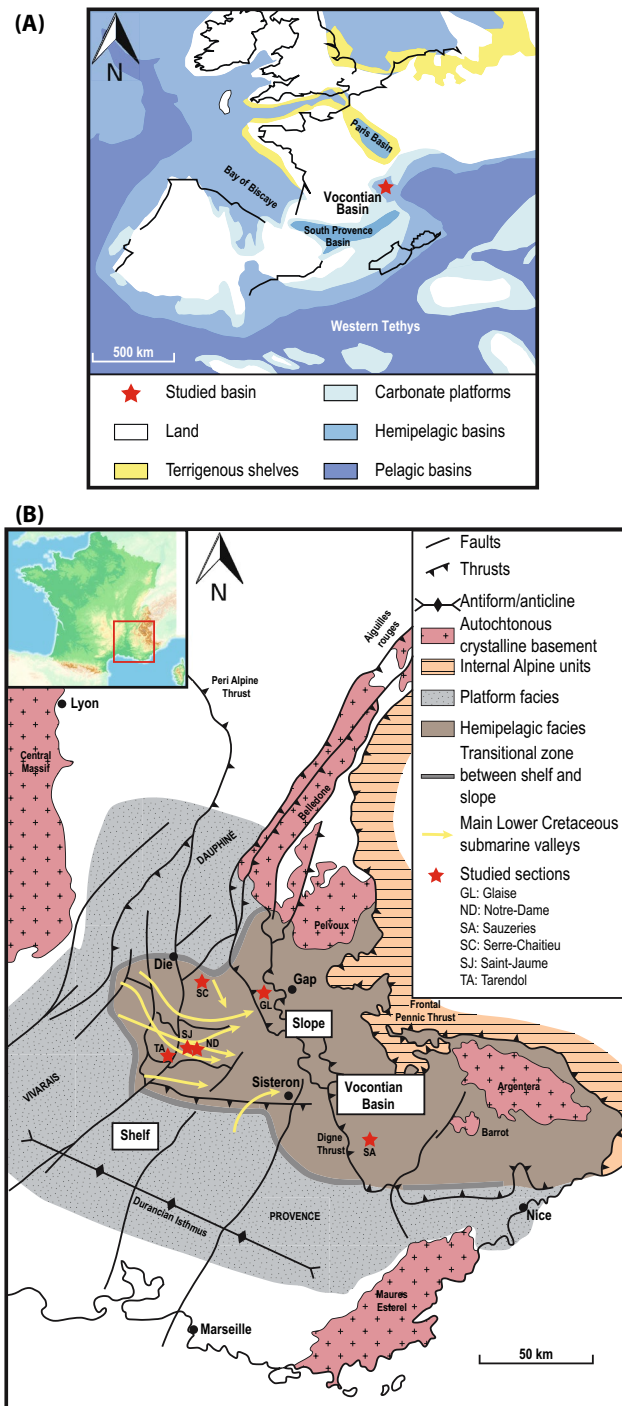


**FIGURE 1** (A) Aptian palaeogeographical map of the western Tethys (in Stein *et al.*, 2012, modified from Masse *et al.*, 2000); (B) Map of the geological context of the Vocontian Basin during Aptian times. The regional settings, main platform limits, submarine valleys and studied sections are displayed (modified from Friès and Parize, 2003)

Western Europe (Bénard *et al.*, 1985; Ziegler, 1990) at the Aptian–Albian boundary (Ferry, 2017). Following this, the Vocontian Basin progressively closed, with the formation of the Pyrenees occurring during the Eocene and the Alps during the Miocene (Baudrimont and Dubois, 1977).

The Vocontian Basin recorded carbonate sedimentation during the Upper Jurassic and Early Cretaceous, but during the Aptian–Albian, terrigenous-dominated sedimentation took place (Friès, 1987; Rubino, 1989; Bréhéret, 1997), giving rise to the marl-dominated hemipelagic facies of the Marnes Bleues Formation that lies stratigraphically above the Barremian/Bedoulian carbonates in the deep part of the Vocontian Basin (Friès, 1987; the Bedoulian being a regional stratigraphic term, corresponding to part of the Lower Aptian). The Marnes Bleues Formation is mainly composed of dark grey marls with low OM content (0.5% on average), with several organic-rich levels (total organic carbon [TOC] > 1.5 wt%) and some carbonate horizons (Tribouvillard, 1989; Bréhéret, 1997). Numerous reworked deposits occur, such as slumps, massive sandstones, turbidites and debris flows, being mainly localized in the north-west part of the basin (Friès, 1987; Rubino, 1989; Friès and Parize, 2003). The thickness of the Marnes Bleues Formation is between *ca* 650 and 800 m (Friès, 1987; Bréhéret, 1997), and the Aptian sediments are 300 m thick. The biostratigraphic framework has been established based on ammonites and foraminifera (Friès, 1987; Bréhéret, 1997; Dauphin, 2002). According to the planktonic and benthic foraminifera biostratigraphy, and palaeodepth estimates deduced from reworked deposit geometries, the palaeobathymetry during the Aptian was estimated to reach *ca* 100 m on the platforms (Arnaud-Vanneau and Arnaud, 1991), and between 500 and 1,500 m on the margin slopes (Beaudoin and Friès, 1984; Arnaud-Vanneau and Arnaud, 1991). During the Albian, the water depth decreased, while the deep part of the basin narrowed, due to the uplifted Provençal Platform as evoked above (Masse and Philip, 1976; Hibschi *et al.*, 1992) coupled with uplift of the western part of the basin (Dauphiné and Vivarais Platforms, Ferry, 2017).

### 3 | THE OAE 1A AND ITS EXPRESSION IN THE VOCONTIAN BASIN

#### 3.1 | General considerations concerning the Early Aptian OAE 1a

The Mesozoic was a time of several major perturbations of the ocean-atmosphere system (Schlanger and Jenkyns, 1976; Jenkyns, 2010). Lasting a relatively short (geological) time (several kyr to a few Myr), OAEs have been related to: (a) intense greenhouse climate conditions; (b) oxygen depletion (reaching anoxic–euxinic conditions) in marine intermediate and/or bottom water masses; and (c) deposition of organic-rich sediments (shales and black shales) in marine hemipelagic to pelagic environments (Schlanger and Jenkyns, 1976;

Arthur and Schlanger, 1979; Arthur *et al.*, 1988; Bralower *et al.*, 1994; Jenkyns, 1999; 2010).

Sedimentation during the Early Aptian was disrupted by the OAE 1a also known as ‘the Selli Episode’ (Coccioni *et al.*, 1987; Arthur *et al.*, 1990; Bralower *et al.*, 1993; Föllmi, 2012). It is now accepted that short phases of exceptionally-intense volcanic activity, accompanying the Ontong Java Plateau Large Igneous Province emplacement in the Western Pacific Ocean, triggered a period of extreme global warming and initiated the OAE 1a (Arthur *et al.*, 1985; Méhay *et al.*, 2009; Tejada *et al.*, 2009; Charbonnier and Föllmi, 2017). Significant biogeochemical changes accompanied the OAE 1a (Föllmi, 2012; Westermann *et al.*, 2013). Prior to the onset of the event, the shallow-water environments on the Tethyan margins were marked by a progressive decline in carbonate production (Föllmi *et al.*, 1994, 2006; Weissert *et al.*, 1998; Huck *et al.*, 2011; Masse and Fenerci-Masse, 2011; Pictet *et al.*, 2015) or by massive occurrences of microbialites (Immenhauser *et al.*, 2005; Huck *et al.*, 2011; Bonin *et al.*, 2016). Moreover, calcareous nannofossil data may indicate acidification of the ocean during the OAE 1a (Erba, 1994; Bralower *et al.*, 1999; Erba *et al.*, 2010; but, see Gibbs *et al.*, 2011). On the other hand, ‘typical’ black shales (laminated, dark-coloured, OM-rich claystones) were deposited in hemipelagic and pelagic environments in numerous locations around the world (see synthesis in Föllmi, 2012). The unfolding of the OAE 1a was favoured by a globally transgressive sea level (Haq *et al.*, 1987; Rubino, 1989; Bréhéret, 1997; Haq, 2014), although a short-lived sea-level fall during the OAE 1a has been proposed (Friès and Parize, 2003; Föllmi, 2012).

From the whole-rock  $\delta^{13}\text{C}$  record of the Cismon section and borehole (central Italy), which is the reference site for OAE 1a deep-water deposits (Weissert *et al.*, 1985; Erba, 1994), the Early Aptian isotope record has been divided into eight segments (C1–C8, Menegatti *et al.*, 1998; Erba *et al.*, 1999). The OAE 1a is characterized by a short negative  $\delta^{13}\text{C}$  excursion (C3 segment, Menegatti *et al.*, 1998), followed by a long, flat positive excursion (Weissert, 1981; Menegatti *et al.*, 1998), supporting intensified volcanic activity as the main trigger of this global carbon cycle perturbation (Menegatti *et al.*, 1998; Méhay *et al.*, 2009). The onset of OAE 1a has been placed at the beginning of the decrease in  $\delta^{13}\text{C}$ , which corresponds to a change in the marine flora and fauna (C4 *p.p.* segment to C6 *p.p.* segment, Bralower *et al.*, 1999; Erba *et al.*, 1999; Méhay *et al.*, 2009; Föllmi, 2012). The biostratigraphic data have been debated, particularly the ammonite biostratigraphy. In most studies, the negative and following positive  $\delta^{13}\text{C}$  excursion correspond to the *Deshayesites deshayesi* ammonite zone (Bréhéret, 1997; Moullade *et al.*, 1998a; Föllmi, 2008, 2012; Masse and Fenerci-Masse, 2011). More recently, the oldest *Deshayesites weissii* ammonite zone (also called *Deshayesites forbesi* in Reboulet *et al.*, 2014)

has been proposed as the datum for the onset of the OAE 1a (Moreno-Bedmar *et al.*, 2009; Malkoc *et al.*, 2010; Frau *et al.*, 2017). The biostratigraphy of OAE 1a is more precisely identified by the *Globigerinelloides blowi* foraminiferal zone and the *Chiastozygus litterarius* nannofossil zone (Bréhéret, 1997). Recent astronomical calibrations have estimated the duration of OAE 1a as being between 1.1 Myr (Malinverno *et al.*, 2010, C4 *p.p.* segment to C6 *p.p.* segment of Menegatti *et al.*, 1998, in the reference core of the Cismon borehole) and 1.4 Myr (Huang *et al.*, 2010, in the Piobbico core, Central Italy).

### 3.2 | Overview of the historical ‘GL’ through the literature

In the deeper parts of the Vocontian Basin (lower slope environment), the GL corresponds to an interval of dark, marly, laminated shales, interbedded with homogeneous, dark, marly shales to marls, dated as Lower Aptian (Bréhéret, 1997). In detail, it corresponds to six horizons of dark, marly, laminated shales (GO 1–GO 6, hereafter called ‘laminated horizons’), rich in OM (TOC up to 5 wt%), each laminated horizon being several centimetres to a metre thick (Bréhéret, 1997). In the literature, these laminated horizons are termed ‘black shales’ (Friès, 1987; Heimhofer *et al.*, 2004; 2006; Okano *et al.*, 2008; Ando *et al.*, 2017) or ‘paper shales’ (Bréhéret, 1994). The GL is synchronous throughout the Vocontian Basin, and the laminated horizons are interbedded with gravity deposits at numerous locations (see below, and also Friès, 1987; Bréhéret, 1997; Friès and Parize, 2003). Recently, the GL was correlated to the OAE 1a based on chemostratigraphic data from the Serre-Chaitieu and Glaise sections (Heimhofer *et al.*, 2004; Westermann *et al.*, 2013). Moreover, the GL is transgressive over the underlying sediments dated as Bedoulian (Lower Aptian *pro parte*; Rubino, 1989). A detailed framework of the GL, and of its six horizons (GO 1–GO 6), has been established within the complete, well-preserved Sauzeries section (Bréhéret, 1997, p. 43, and Figure 2). Few complete, entire, well-preserved successions are observed in the Vocontian Basin; however, the GO 5 horizon is recognizable across all the sections (Bréhéret, 1997). The thickness of the GL can vary from 4.3 m in a section without gravity deposits (the Sauzeries section, Figure 2) to about 17 m when gravity deposits are present (turbidites and slumps in the Saint-Jaume section, Figure 1; Bréhéret, 1997; Friès and Parize, 2003). The sections cited below are shown on Figure 1.

In the proximal parts of the Vocontian Basin (proximal slope environment), the GL was deposited only on the western border, interbedded with thin turbidites (Rubino, 1989; Bréhéret, 1997). On the platform, due to intensive currents (Cotillon, 2010), there is no sediment corresponding to the

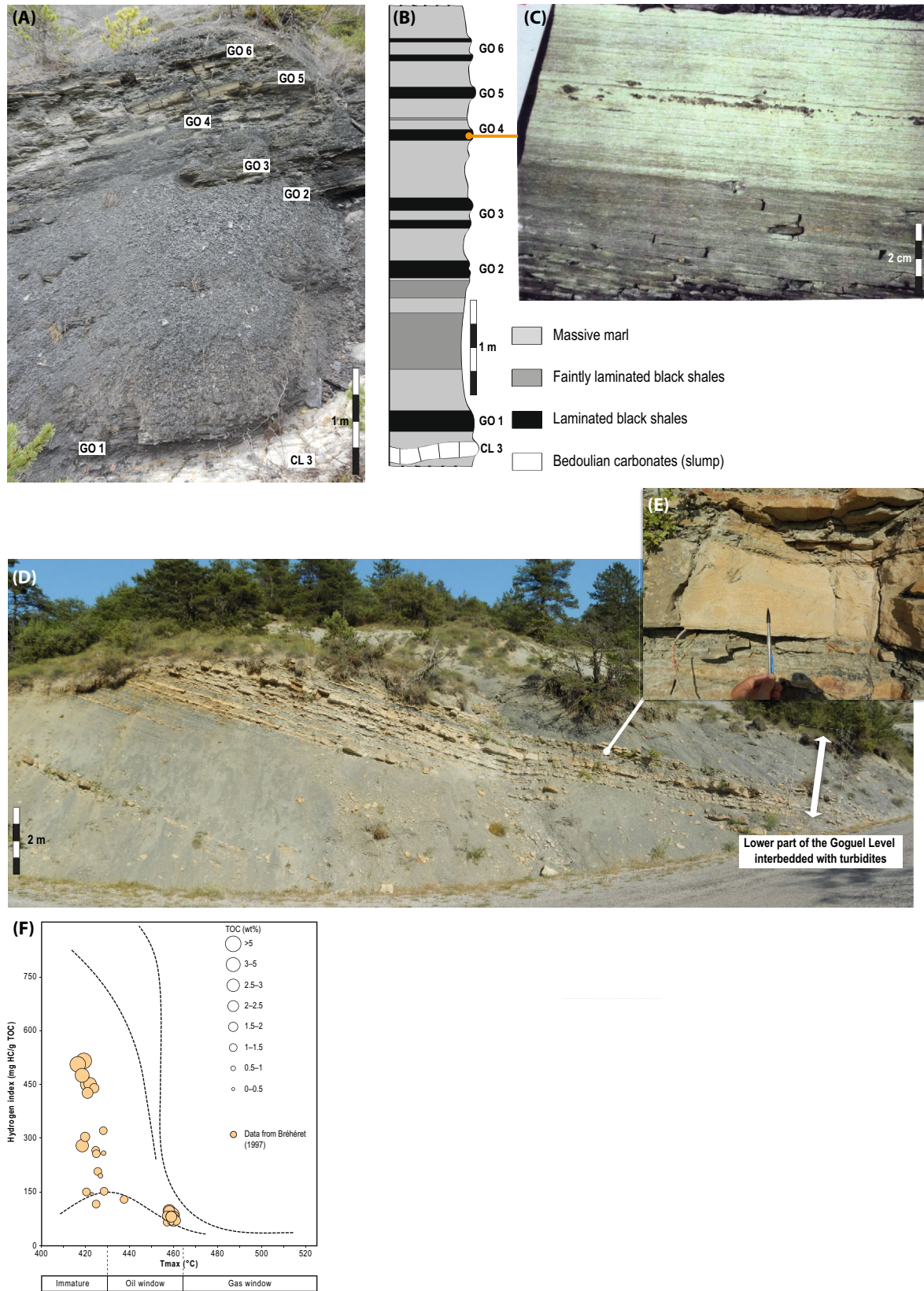


**FIGURE 2** (A) Sauzeries section with the well-preserved six horizons of the GL (GO 1–GO 6). (B) Sauzeries log-section (from Bréhéret, 1997). (C) Example of the lithology in one laminated horizon of the GL, the GO 4 level (picture from Bréhéret, 1997). (D) Example of the GL interbedded with thin turbidites, Notre-Dame section. (E) Tb and Tc members (sensu Bouma, 1962) of a thin turbidite within the GL in the Notre-Dame section, showing a normal grading with the gradual transition between planar and convolute laminations, pencil = 15 cm. (F) HI-Tmax diagram showing the typology of the OM in the GL (diagram from Espitalié *et al.*, 1985; data from Bréhéret, 1997)

GL, and the OAE 1a has been interpreted as being represented by a hiatus (Frau *et al.*, 2017), with a few phosphatic remains of ammonites in the Nice area possibly recording the OAE 1a (Bréhéret, 1997). Near Marseille, the GL corresponds to homogeneous grey marls *ca* 10 m thick (Cassis-La Bédoule section, Moullade *et al.*, 1998b; Stein *et al.*, 2012).

The GL contains few macrofossils (rare ammonites and fish fragments), but is rich in foraminifera (Bréhéret, 1997). According to Bréhéret (1997 and references therein), the GL pertains to the *D. deshayesi* ammonite zone and the *G. blowi* planktonic foraminifera zone, although this time interval is poorly constrained in the Vocontian Basin. Moreover, the upper part of the GL is marked by the base of the *Rhagodiscus angustus* calcareous nannofossil subzone (NC7A, Herrle and Mutterlose, 2003) and by the top of the *C. litterarius* calcareous nannofossil zone (NC6). With the exception of the laminated horizons, the sediments of the GL are intensely bioturbated by a low-diversity ichnofauna (dominated by *Chondrites* with rare *Planolites*; Bréhéret, 1997). The laminated horizons are rich in faecal pellets, with no benthic fauna (Bréhéret, 1997; Dauphin, 2002).

On average, the carbonate content in the Marnes Bleues Formation ranges between 25% and 35%. The lowest contents are in the GL, particularly in the marls hosting the laminated horizons (10%–15% after Bréhéret, 1997; 12%–36% after Heimhofer *et al.*, 2004). The poor preservation of bioclasts (calcareous nannofossils and foraminifera) and the low planktonic foraminifera content (compared to the rest of the Marnes Bleues Formation) likely account for the low carbonate content. The decrease in carbonate production in the Vocontian Basin has been attributed to a change in the oceanic environment (Bréhéret, 1997).

The GL contains 30%–50% clay-sized grains (<2  $\mu\text{m}$ , Bréhéret, 1997). The clay mineral distribution in the terrigenous fraction is dominated by illite, smectite and illite–smectite mixed-layer minerals. According to various authors, the proportions of these clay minerals are variable, each representing 20%–30% of the <2  $\mu\text{m}$  fraction (Deconinck, 1984; Bréhéret, 1997; Ghirardi *et al.*, 2014). Kaolinite and chlorite represent less than 10% each of the fine-grained fraction.

Redox-sensitive elements (Mo, U, Cr and Co; Westermann *et al.*, 2013) yield a very moderate enrichment relative to the post-Archean average shale values in the Glaise section (Taylor and McLennan, 1985). Productivity proxies (Ni, Cu) also indicate a slight enrichment during the GL (Westermann *et al.*, 2013). Moreover, U–Mo covariations have been interpreted as corresponding to an unrestricted suboxic marine environment. Furthermore, the discovery of a Ce anomaly (Ce/Ce\*) in the Glaise section supports low-oxygenation conditions during deposition of the GL (Bodin *et al.*, 2013).

According to the literature (Tribouillard, 1989; Bréhéret, 1994; 1997; Heimhofer *et al.*, 2004, 2006; Westermann *et al.*, 2013; Ando *et al.*, 2017), the TOC of the GL fluctuates between

0.5 and 5 wt%. For the laminated horizons (GO 1–GO 6), the contents range between 2 and 5 wt%. The Hydrogen Index (HI) reaches up to 500 mgHC/gTOC, ascribing the GL OM to Type-II kerogens (marine OM field) in a HI-Tmax diagram (Figure 2, Espitalié *et al.*, 1985). The Tmax values of the GL samples vary (420–440°C, Bréhéret, 1997; Westermann *et al.*, 2013), but they indicate in a HI-Tmax diagram that the OM is in an immature state (Figure 2). In the Cassis-La Bédoule section, the TOC values are very low (<0.5 wt%; Stein *et al.*, 2012), and the OM is ascribed to Type-III kerogens (terrestrial OM field); because of the very low TOC, the HI cannot be taken into account in a HI-Tmax diagram (Espitalié *et al.*, 1985). Molecular biomarker analysis of the GL OM from the Serre-Chaitieu section has indicated a significant contribution from marine algal-bacterial OM, based on the distribution of linear alkanes (*n*-alkanes) and tetra and pentacyclic terpanes (Heimhofer *et al.*, 2004). These authors suggested a minor contribution of terrestrial OM based on the low abundance of long-chain *n*-alkanes. A study of the palynofacies of the Serre-Chaitieu section revealed that the GL was mainly composed of marine-derived OM (Heimhofer *et al.*, 2006). The kerogens of the laminated horizons are constituted of approximately 95% highly fluorescing amorphous OM, while the host dark marls contain 70%–80% amorphous OM (Heimhofer *et al.*, 2006). Phytoclasts represent 40% of the particulate OM, and abundant small (<20  $\mu\text{m}$ ), equidimensional phytoclasts, coupled with small, oxidized fragments and charcoal debris, indicate that terrestrial OM only slightly contributes to the total OM deposited in this quiet and distal environment (Heimhofer *et al.*, 2006). These environmental observations are consistent with the predominance of dinoflagellate cysts in the kerogen extracts (Heimhofer *et al.*, 2006). Furthermore, the unchanged colour of the palynomorphs, and the moderate to high UV fluorescence of the amorphous OM and palynomorphs, confirm the low maturity of the OM in the GL (Heimhofer *et al.*, 2006).

According to numerous authors (Friès, 1987; Rubino, 1989; Bréhéret, 1997; Friès and Parize, 2003; Westermann *et al.*, 2013), the GL is partly reworked (slump  $\beta$  of Friès, 1987; Friès and Parize, 2003), or is interbedded with millimetre to multi-centimetre thick turbidites (P1 turbidites of Rubino, 1989). Slump  $\beta$  is 10 m thick over an area of 40 km<sup>2</sup> (Friès and Parize, 2003). The P1 turbidites correspond to ‘classical’ turbidites (*sensu* Bouma, 1962), according to the study of Friès and Parize (2003) (Figure 2). They are mainly composed of Tb to Te members (Friès and Parize, 2003, Figure 2). The P1 turbidites are metre-thick packages and are distributed over 80 km along the ancient margin (Rubino, 1989; Friès and Parize, 2003). The submarine canyons filled by these turbidites had a width of a few hundred metres (Friès and Parize, 2003). The turbidites correspond to the destabilization of a small amount of sand stored on the platform during the global sea-level transgression associated with the OAE 1a

(Rubino, 1989; Br  h  ret, 1997). For a long time the turbidites have been closely associated with the GL (Fri  s, 1987; Rubino, 1989; Br  h  ret, 1994, 1997) and are interbedded within the homogeneous, dark, marly shales to marls, or lie just above the laminated horizons, but never at the base of, or within these laminated horizons (Br  h  ret, 1997). Moreover, according to Br  h  ret (1997): (a) the enrichment and quality of the OM observed in the sections is similar, with or without turbidites and (b) the laminated horizon GO 5, which is the most widely represented in the basin, has approximately the same expression and thickness at several basin locations, with or without turbidites. These observations suggest that the turbidites did not trigger the deposition or enrichment of the OM content of the GL (Br  h  ret, 1997); it was only turbidity currents disturbing the settling of fine particles in this quiet pelagic environment (Br  h  ret, 1997).

Previous studies allowed the depositional conditions to be constrained for the GL. Several parameters indicate suboxic to anoxic conditions for the laminated horizons: (a) the occurrence of undisturbed laminations, and therefore the lack of bioturbation (Br  h  ret, 1997); (b) the lack of a benthic fauna in the laminated horizons (Br  h  ret, 1997); (c) an ichnofauna dominated by *Chondrites*, characteristic of a quiet environment with low oxygenation (Br  h  ret, 1997); (d) the distribution of redox-sensitive trace elements and a Ce anomaly (Bodin *et al.*, 2013; Westermann *et al.*, 2013); (e) the good preservation of marine-derived OM, and the abundance of highly fluorescent amorphous OM in the palynofacies (Heimhofer *et al.*, 2006).

In addition to the oxygenation conditions, OM enrichment of the GL could have been impacted by the sedimentation rate (SR). Thus, condensation seems to be one of the key factors responsible for OM enrichment during sedimentation of the GL (Br  h  ret, 1994, 1997; Heimhofer *et al.*, 2006). The role of condensation is highlighted by the high TOC correlated with: (a) peaks in carbonate content (indicating reduced influx of land-derived particles, Br  h  ret, 1994); (b) peaks in palynomorph abundances in the palynofacies (indicating weak hydrodynamism in the transport of particulate OM, Heimhofer *et al.*, 2006); and (c) low SRs (Westermann *et al.*, 2013).

In summary, the sedimentation and preservation of OM in the GL are related to a global sea-level transgression (Haq *et al.*, 1987; Haq, 2014; confirmed by regional studies; Rubino, 1989; Br  h  ret, 1997; Ferry, 2017), with generally low oxygenation of the deep-water mass (Br  h  ret, 1997; Heimhofer *et al.*, 2006; Westermann *et al.*, 2013), coupled with a significant period of sedimentary condensation (Br  h  ret, 1997; Heimhofer *et al.*, 2006).

Nevertheless, some problems limit the understanding of the depositional environments of the GL. First, what was the primary factor that induced OM enrichment in the GL? For some authors (Br  h  ret, 1997; Heimhofer *et al.*, 2006), primary productivity was not the key factor (it was instead

condensation coupled to anoxia), whereas Westermann *et al.* (2013) attributed a significant role to surface-water productivity, especially as a precursor to the OAE 1a. Second, the impact of possible climate change on the Vocontian Basin is still under debate. Several studies agreed that higher temperatures and humidity existed during deposition of the GL (Stein *et al.*, 2012; Bodin *et al.*, 2013; Westermann *et al.*, 2013; Ghirardi *et al.*, 2014), involving increased runoff, although this seems to be inconsistent with the period of condensation observed in the basin. Contrarily, other studies have proposed that there was no major climate change during deposition of the GL (Br  h  ret, 1997; Heimhofer *et al.*, 2004). Although major climate change has been hypothesized for the Tethys Ocean during the Early Aptian OAE 1a (F  llmi, 2012 and references therein), its expression was perhaps less perceptible in the Vocontian Basin. Third, oxygenation conditions in the basin during the OAE 1a must be better defined. In order to improve the depositional model of the GL four sections, located in contrasting palaeo-settings in the Vocontian Basin, were analysed using a multi-proxy approach.

## 4 | MATERIALS AND METHODS

### 4.1 | Sampling and sections

For this study, 77 samples were analysed from six sections in the Marnes Bleues Formation. Thirty-two samples of the GL (ending with the suffix ‘-g’) were taken from four sections. These sections were situated at different locations in the Vocontian Basin: the Saint-Jaume and Notre-Dame sections are on the palaeo-upper slope, while the Glaise and Sauzeries sections correspond to the palaeo-lower slope of the basin (Figure 1). In order to facilitate interpretation and characterization of the GL, 45 samples of the so-called Aptian Hemipelagites (AHs; ending with ‘-h’) were collected. These hemipelagites correspond to the background sedimentation in the Vocontian Basin during the Aptian.

The Glaise section (Figure 1, WGS 84 coordinates: 44  34’07.2’’N, 5  49’01.6’’E) is located about 20 km west of the city of Gap, in Veynes town. There, the GL is represented by a 12.7 m thick interval, interbedded with centimetre-scale turbiditic layers, underlying the marly limestone beds at the top of the section (Br  h  ret, 1997). The Sauzeries section (Figure 1, 44  02’01.1’’N, 6  21’28.4’’E) is located in the town of Clumanc, *ca* 10 km south-east of the city of Digne-les-Bains. There, the GL is 4.3 m thick (Br  h  ret, 1997). The Saint-Jaume section (Figure 1, 44  22’59.9’’N, 5  26’17.9’’E) is located *ca* 20 km east of the city of Nyons, in the town of Verclause. At the base of a thick marly section (>150 m), the GL is interbedded with numerous centimetre-scale turbiditic layers within slump   , over a thickness of 17 m (Br  h  ret, 1997; Fri  s and Parize, 2003). The Notre-Dame section (Figure 1, 44  23’30.7’’N, 5  29’58.3’’E) is

located in Saint-André-de-Rosans, *ca* 25 km west of the city of Serres; however, only the base of the GL was observed there, interbedded with centimetre-scale turbiditic layers (example on Figure 2; Friès and Parize, 2003). Because the GL thickness has not been determined, no SR has been calculated for this section; nevertheless, the thickness is at least greater than 5 m. The Serre-Chaitieu section (Figure 1, 44°35'24.0"N, 5°32'00.2"E) is located in Lesches-en-Diois *ca* 40 km west of the city of Gap, and the Tarendol section (Figure 1, 44°21'08.0"N, 5°20'44.4"E) is located in Bellecombe-Tarendol, *ca* 15 km east of the city of Nyons. Although the GL occurs in these sections, only the AHs were sampled.

For each sample, 500 g to 1 kg of rock were collected. To avoid contamination of the sediment by plastic or cardboard, the samples were stored in aluminium foil. Considering the SRs and duration of the GL (see below), each of these relatively thick samples correspond to several thousand years of sedimentation, contrary to existing highly accurate studies on the timing and environmental changes occurring during the OAE 1a (Menegatti *et al.*, 1998; Erba *et al.*, 1999, 2015; Heimhofer *et al.*, 2004; Bottini *et al.*, 2015; Giraud *et al.*, 2018).

## 4.2 | Grain-size analysis

Grain-size analysis was performed on the carbonate-free fraction of 76 samples, using a Malvern Mastersizer 2000<sup>®</sup> laser diffractometer, at the Laboratoire d'Océanologie et de Géosciences (LOG) of Lille University, following the classical protocol detailed in Trentesaux *et al.* (2001). The uncertainty in the values is *ca* 5% (Sperazza *et al.*, 2004), and for the finest grain sizes—clay-sized particles of <5 µm—the apparatus slightly minimizes the abundance (by a few %) according to the manufacturer. The grain-size scale used is clay (<2 µm), fine or cohesive silt (2–10 µm), coarse or non-cohesive silt (10–63 µm) and sand (63–2,000 µm). According to McCave *et al.* (1995), silts (2–63 µm) should be separated based on the behaviour of the particles—if they are thinner than 10 µm, they behave in a similar manner as clay (cohesive silts), whereas silts coarser than 10 µm (sortable silts) behave as single particles, influenced by hydrodynamic forces during erosion and deposition (non-cohesive particles). Coarser silts were used as current-strength indicators (McCave *et al.*, 1995). Lastly, the fraction below 2 µm (and not 4 µm) was considered to be clay because the clay mineral assemblage determination was carried out on the <2 µm fraction.

## 4.3 | Clay minerals

For the <2 µm terrigenous fraction, clay mineral assemblages were analysed in 77 samples using standard X-ray diffraction

protocol (Brucker D4 ENDEAVOUR apparatus in the LOG, Lille University) described in detail in Bout-Roumazelles *et al.* (1999). Semi-quantitative estimates of clay mineral abundance, the Kübler Index (illite crystallinity) and the Esquevin Index (chemical weathering index) were all determined using MacDiff<sup>®</sup> 4.2.5 software, according the methodology of Riboulleau *et al.* (2014). The Kübler Index is inversely proportional to the degree of metamorphism (Kübler, 1967; Kübler and Jaboyedoff, 2000). The Esquevin Index allows Al-rich illite to be differentiated from Mg-rich illite (Dunoyer de Seconzac, 1969; Esquevin, 1969) and, therefore, may help to detect strong hydrolysis on an emerged source area that would favour the high proportion of magnesian illite mirrored by the high Esquevin Index. The relative margin of error for a semi-quantitative estimation was ±5% (Bout-Roumazelles *et al.*, 1999). In order to evaluate the possible relationship between the sedimentation of OM and the occurrence of clay minerals, the proportions of clay minerals in the sediments were estimated using the following formula:

$$\begin{aligned} &\text{Bulk \% clay mineral} \\ &= (\% \text{ clay mineral in terrigenous clay fraction}) \\ &\times (100 - \text{CaCO}_3 (\%)) \\ &\times (\% \text{ clay fraction } (<2\mu\text{m}) \text{ in the terrigenous fraction}). \end{aligned}$$

## 4.4 | Rock-Eval

Seventy seven samples were evaluated using Rock-Eval 6<sup>®</sup> pyrolysis (see Behar *et al.*, 2001 for details) at the Sorbonne Université (ISTeP, Paris). The TOC (wt%), HI (mg HC/g TOC), oxygen index (OI, mg CO<sub>2</sub>/g TOC) and Tmax (°C, indicator of OM thermal maturity) were determined. According to Espitalié (1993), Rock-Eval pyrolysis parameters allow the type and thermal maturity of bulk OM to be typified. Bearing in mind that the carbonate fraction of the Marnes Bleues Formation is mainly calcite (Bréhéret, 1997), the total carbonate content (CaCO<sub>3</sub>, in %) was calculated from the Rock-Eval MinC (%), using the formula of Jiang *et al.* (2017):

$$\text{CaCO}_3 (\%) = 7.976 \times \text{MinC} (\%).$$

## 4.5 | Elemental analysis

Major and trace element contents of the Glaise (*p.p.*) and Sauzeries sections (24 samples) were determined at the University of Lausanne (ISTE-UNIL laboratory) using X-ray fluorescence spectrometry, according to the protocol detailed in Montero-Serrano *et al.* (2015). The detection limits were <0.01 wt% for major elements, and between 1 and 5 ppm for trace elements. The accuracy of the analysis was checked by the analysis of standard reference materials.

For the Notre-Dame, Glaise (*p.p.*), Saint-Jaume, Serre-Chaitieu and Tarendol sections (45 samples), major and trace element analyses were performed at Central Michigan University in the STARLAB Laboratory, using inductively coupled plasma mass spectrometry, and external calibration. Analytical precision, based on replicate analyses, was better than 8%, and detection limits were <1 ppb for the major elements and <40 ppt for the trace elements.

In order to compare the distributions of elements among sections, enrichment factors (EFs) were calculated:

$$X_{EF} = (X/Al)_{\text{sample}} / (X/Al)_{\text{upper crust}}$$

where X and Al are the concentrations of element X and Al (wt%), EFs are normalised using the elemental upper crust concentrations of McLennan (2001) and, to minimize the effects of dilution by carbonate or biogenic silica, Al normalisation is commonly used (see Tribovillard *et al.*, 2006 for explanations and limits). Detectable enrichment of an element above average upper crustal concentrations corresponds to an EF > 3, while a moderate to strong enrichment represents an EF > 10 (Algeo and Tribovillard, 2009).

In addition, a chemical weathering index—the Index of Alteration (IA)—was calculated. The IA is equivalent to the Chemical Index of Alteration (CIA, Nesbitt and Young, 1982), but, in carbonate-rich sediments (>30% carbonates), the CIA can give misleading data (Goldberg and Humayun, 2010). Thus, a compositional linear trend, as proposed by Von Eynatten *et al.* (2003), can be used as a CIA equivalent (Montero-Serrano *et al.*, 2015):

$$IA = \text{LN} (Al_2O_3/Na_2O), \quad \text{in molar proportions.}$$

This index avoids uncertainties concerning the necessary corrections for non-silicate phases, in particular carbonate and phosphate phases (Von Eynatten *et al.*, 2003). An increase in IA values can be interpreted as more intense chemical weathering within the sediment-supplying, emerged source areas.

#### 4.6 | Average SR and total organic carbon mass accumulation rates

According to Heimhofer *et al.* (2004), because the SRs calculated by Köbller *et al.* (2001) ranged between 3.0 and 3.5 cm/kyr in the lower part of the Upper Aptian (regardless of compaction rates), the SRs of the GL (which corresponded to a period of condensation) were probably between 2.0 and 2.5 cm/kyr; however, the SRs calculated from the Glaise section (0.67–2.3 cm/kyr, Westermann *et al.*, 2013) were probably less than 2.0–2.5 cm/kyr. The method of Westermann *et al.* (2013) was used to calculate the SRs of the Glaise section, using a combination of  $\delta^{13}C$

chemostratigraphy and orbital calibrations; the other sections studied do not have  $\delta^{13}C$  data. However, it was possible to calculate an average SR where the GL was entirely present in the outcrop (which is the case for the Glaise, Saint-Jaume and Sauzeries sections) using the orbital calibrations of Malinverno *et al.* (2010). The Early Aptian OAE 1a is estimated to have lasted for  $1.11 \pm 0.11$  Myr (Malinverno *et al.*, 2010). The average SRs were calculated by:

$$\text{Average SR (cm/kyr)} = \text{thickness of GL} / \text{duration of OAE 1a,}$$

where the thickness of GL was measured in centimetres and the duration of OAE 1a was estimated to be 1,110 kyr (Malinverno *et al.*, 2010). In the Serre-Chaitieu section, the average SR of the AHs samples in the Fallot interval, which corresponds to numerous bundles of two or three horizons of dark marlstones in the Upper Aptian (Bréhéret, 1997; Dauphin, 2002), was calculated using the orbital calibrations of Huang *et al.* (2010).

In order to evaluate variations in organic carbon input, the TOC mass accumulation rate (TOC MAR) was calculated following the approach developed by Westermann *et al.* (2013) for the Glaise section:

$$\text{TOC MAR (mg/cm}^2\text{/kyr)} = (\text{TOC (wt\%)} \times \text{rock density (g/cm}^3\text{)} \times \text{average SR (cm/kyr)}) \times 10$$

where the TOC values come from Rock Eval data, the rock density is 2.3 and 2.4 g/cm<sup>3</sup> for marlstones and siltstones, respectively (Attewell and Farmer, 1976, marlstones if CaCO<sub>3</sub> (%) > 35%), and the average SR was calculated using the previous formula. This useful accumulation rate was also calculated in the present study.

It is important to note that the intent of calculating these accumulation rates (average SR and TOC MARs) is to allow the sections to be compared amongst each other; any direct comparison with accumulation rates in modern environments, or other geological formations, is tricky because the compaction rate is not considered here in the average SR. In addition, the duration of the GL was considered to be the same as the duration of the OAE 1a, because there is no precise duration for the GL available in the literature (Westermann *et al.*, 2013; Giraud *et al.*, 2018).

#### 4.7 | Molecular biomarkers

Twenty-four samples were selected for biomarker analysis. Between 50 and 70 g of dry sediments were extracted using an azeotrope mixture of dichloromethane (DCM) and methanol (MeOH) 2:1 v/v, by means of a soxhlet extractor for 48 h. The resulting total extract was rotary-evaporated to dryness at a temperature not exceeding 50°C. The extracts were recovered with cyclohexane (maltenes), and separated

over an activated silica column, using cyclohexane (Cy) to recover the aliphatic fraction, a mixture of Cy/DCM 2:1 (v/v) to recover the aromatic fraction, and a mixture of DCM/MeOH 2:1 (v/v) to recover the most polar fraction.

Analyses were performed at the University of Lille, France (PC2A Laboratory UMR 8522 CNRS), by injecting 1  $\mu$ l of extract into a gas chromatograph (Perkin Elmer 680) coupled with a mass spectrometer (Perkin Elmer 600C). The chromatographic conditions were: inlet heated to 250°C; DB5-MS-UI column initially at 40°C for 1 min, then heated to 320°C at 10°C/min, and maintained for 10 min at 320°C; and helium column flow of 1 ml/min, in split less mode. The mass spectrometer conditions were: mass scan 45 e 500; scan time 0.2 s; interdelay scan 0.1 s; and ionization energy 70 eV. For the purpose of product semi-quantification, standard solutions of 2,2,4,4,6,8,8-heptamethylnonane, anthracene D10 and C<sub>29</sub>-nonadecanone (Dr. Ehrenstorfer-Shäfers, Augsburg, Germany) were used. The identification of compounds was based on comparison with the NIST mass spectra database and/or comparison with retention times of standards and published data. Quantification was achieved by measuring the peak area of the compounds selected in several ion chromatograms.

## 5 | RESULTS

All data are available upon request. Moreover, boxplots are used (Figure 3) in order to facilitate the comparison between the AHs and the GL.

### 5.1 | Bulk organic matter

Rock Eval pyrolysis of the AHs display an average TOC of 0.6 wt% (ranging from 0.21 to 1.31 wt%), while the GL have a TOC ranging from 0.25 to 7.26 wt%, with an average of 1.9 wt%. The moderate enrichment of OM in the GL, compared to the AHs, is also confirmed by the differences in the S1 and S2 data: (a) 0.03–1.71 mg/g and 0.01–0.10 mg/g respectively for S1; and (b) 0.21–37.76 mg/g and 0.16–1.99 mg/g respectively for S2. Moreover, the range of HI values in the GL (66–520 mgHC/gTOC, average of 275 mgHC/gTOC) are clearly higher than those of the AHs (27–209 mgHC/gTOC, average of 71 mgHC/gTOC), while the OI data are substantially higher in the AHs than in the GL (average of 63 mgCO<sub>2</sub>/gTOC and 23 mgCO<sub>2</sub>/gTOC, respectively). The *T*<sub>max</sub> data of the GL (ranging from 425 to 441°C, average of 435°C) are slightly higher than those of the AHs (ranging from 425 to 436°C, average of 430°C). Because the majority of samples (76 out of 77) display a TOC > 0.3 wt%, the HI and OI parameters could be interpreted in a HI-*T*<sub>max</sub> diagram (Figure 4, Espitalié *et al.*, 1985). The AHs show predominantly Type-III kerogen

(terrestrial OM field), while the GL of the Saint-Jaume and the Glaise sections shows Type-II-III kerogens (mixed terrestrial-marine OM). In the Notre-Dame and Sauzeries sections, the GL exhibits distinctly type-II kerogens (marine OM field). All the *T*<sub>max</sub> values indicate an immature stage to oil window stage for the kerogens. The carbonate contents are very variable (1%–80%), with an average of 21% in the GL and an average of 36% in the AHs.

In the GL, the TOC is relatively constant, except for the Sauzeries section (Figure 3). Indeed, the average TOC of the Sauzeries section (3.3 wt%) is three times higher than in the other sections (approximately 1 wt% on average). The same trend is observed for HI values that are higher in the Sauzeries section (387 mgHC/gTOC) compared to other sections (around 200 mgHC/gTOC, Figure 3). The *T*<sub>max</sub> values are slightly higher in the distal sections than in the proximal sections. Furthermore, the carbonate contents are slightly higher in the Sauzeries section (26% on average, Figure 3) than in the other ones (average carbonate content in Saint-Jaume section is 25%, but skewed by one high value).

### 5.2 | Grain-size

The sediments of the Marnes Bleues Formation mainly correspond to siltstones (carbonate content <35%) and marlstones (carbonate content >35%). The mode of the grain-size distribution is very variable, ranging from 8 to 76  $\mu$ m. The GL shows an average mode slightly lower than that of the AHs (24 and 33  $\mu$ m, respectively, which cannot be accounted for by the organic-particle content with TOC values so low). In the GL and AHs samples, the distribution of particle sizes follows a unimodal normal distribution. The distribution of the grain-size classes is approximately the same for the two groups: 1% on average for clays; about 30% on average for the cohesive silts (33% for the GL, 29% for the AHs); a predominance of sortable silts (56% on average for the GL; 58% for the AHs); and about 10% on average for the sands (10% for the GL; 12% for the AHs). The difference between the two groups is observable within the bulk sediment fraction (terrigenous and carbonate fractions). Indeed, the clay and the sand classes are the same for the two groups (<1% and 8%, respectively), but, on the other hand, the silt classes show some dissimilarity. Thus, the GL contains on average more cohesive and sortable silts (26% and 44%, respectively) than the AHs (18% and 37%, respectively).

The grain-size data within the GL show little variation. The silt content (cohesive and sortable) is higher in the Glaise section (85% on average) while the sand content of the distal sections is lower than that of the proximal sections (Figure 3). Moreover, the mode values of proximal sections are more scattered than those of distal sections (Figure 3). Lastly, no variations were observed in the percentage of clay grade material.

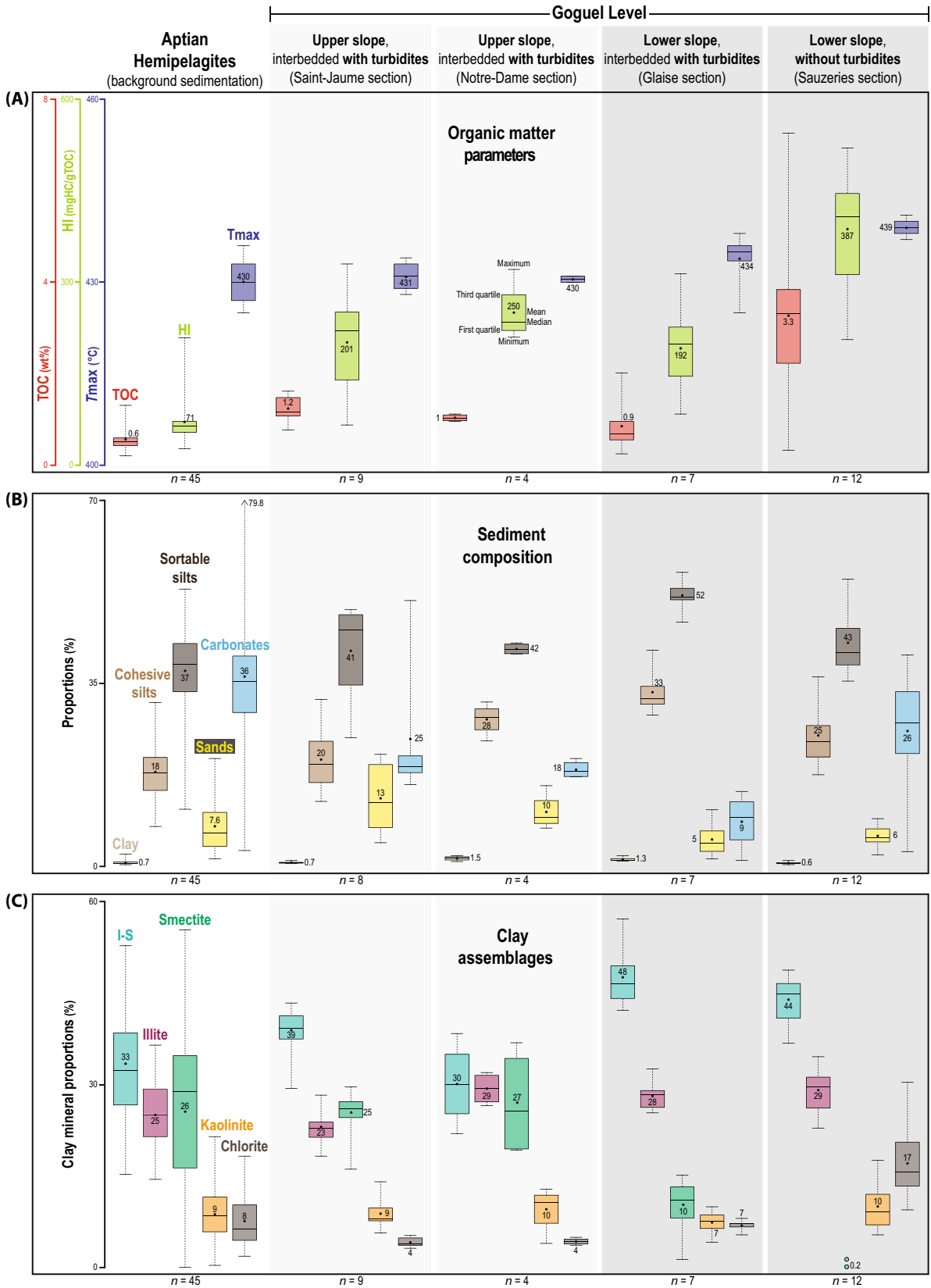


**FIGURE 3** Boxplots of (A) organic matter parameters; (B) sediment composition; (C) clay assemblages. The legend of boxplots is show in the HI boxplot of the Notre-Dame section. Boxplots of (D) Redox-sensitive elements; (E) Productivity-sensitive elements and index of alteration; and (F) Mode and accumulation rates. The legend of boxplots is show in the HI boxplot of the Notre-Dame section

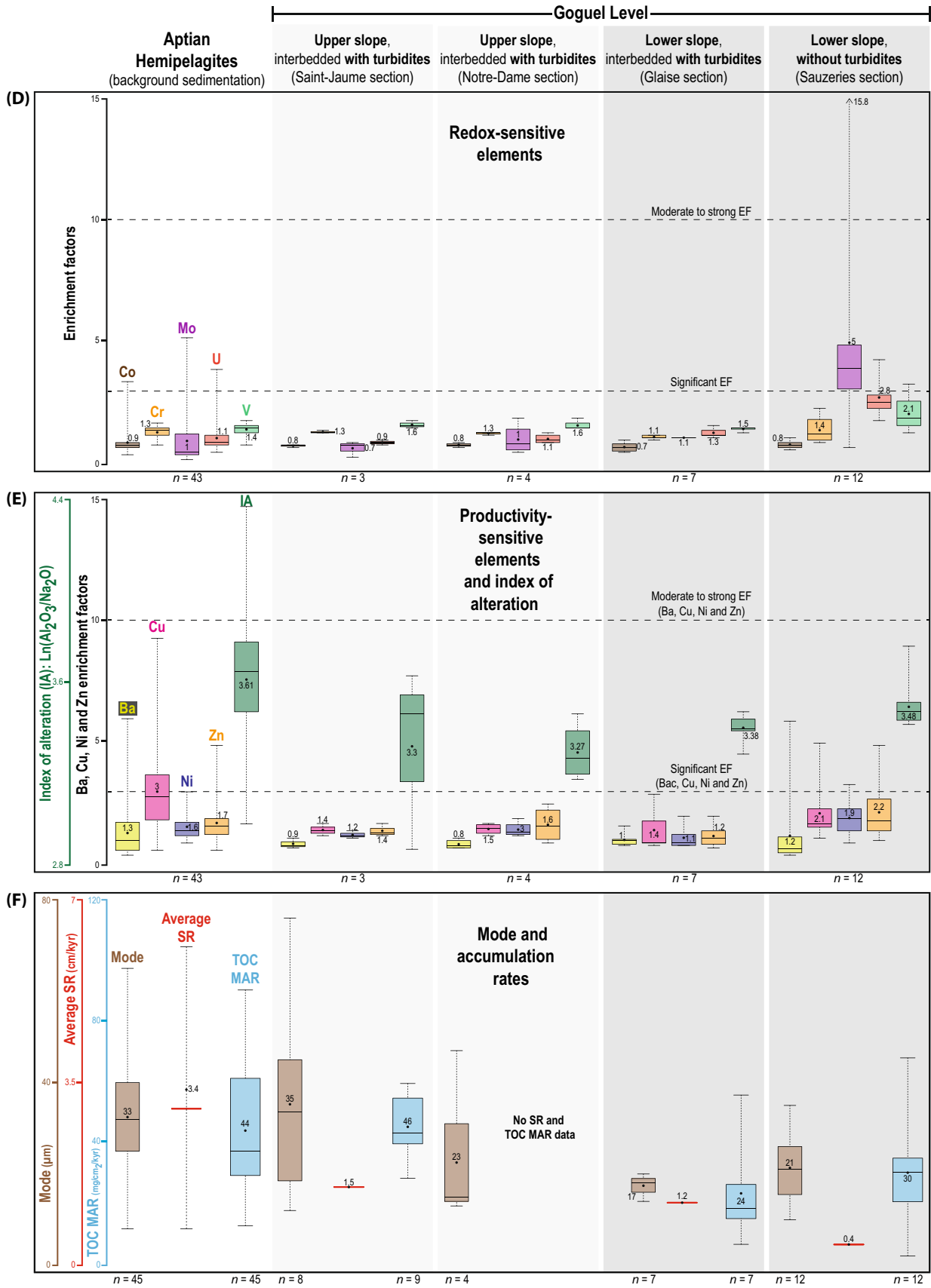
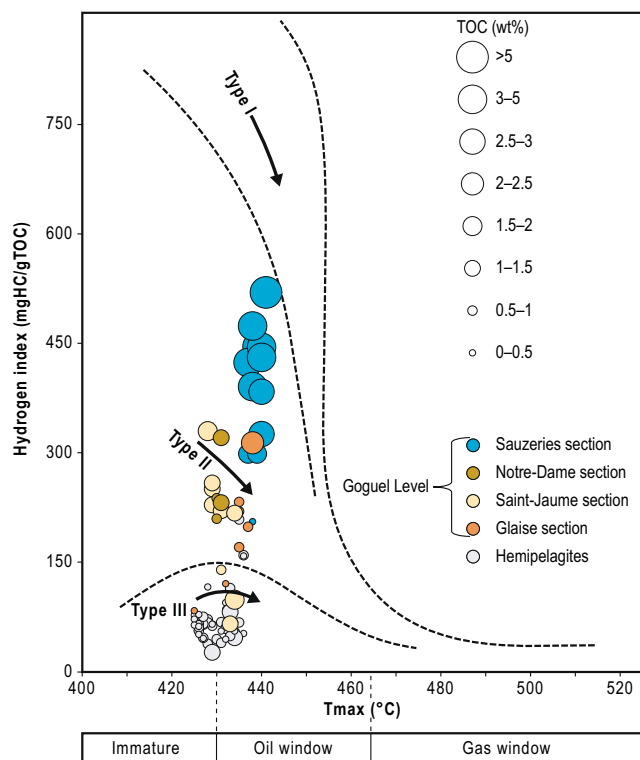


FIGURE 3 continued



**FIGURE 4** HI-Tmax diagram showing the typology of the OM for the studied samples (diagram from Espitalié *et al.*, 1985)

### 5.3 | Clay minerals

The distribution of clay minerals is dominated by the illite-smectite mixed-layers (I-S; corresponding to irregular I/S R0 type interstratified clay minerals with more than 50% layers of smectite; Chamley, 1989), illite and smectite in decreasing proportions. The GL shows high contents of I-S (42% on average) and illite (average of 27%). In the same way, the AHs have high average contents of I-S (33%) and illite (25%). The main difference is observed in the average contents of smectite: 13% for the GL, against 26% in the AHs. However, the average value of the GL is clearly impacted by the lack of smectite in the Sauzeries section. In the other sections (Glaise, Notre-Dame and Saint-Jaume), the average content of smectite is 20%. Kaolinite and chlorite are present in low proportions (less than 10% on average within the GL and the AHs).

In the GL, an increase in the amount of illite is observed in distal sections (about 45% on average, Figure 3). Conversely, the smectite content decreases in the distal locations of the Glaise section (10% on average) and is essentially lacking in the Sauzeries section (only 2 samples with 2 and 0.4%). The I-S, kaolinite and chlorite contributions are constant between the sections, except for a peak of chlorite in the Sauzeries section (17% on average, Figure 3).

In order to evaluate the relative abundance of clay minerals in the sediment, the clay mineral content of bulk sediment

has been calculated. Because the clay contribution is very small in the terrigenous fraction (<1%), the bulk proportions of I-S, illite and smectite minerals are extremely low (0.20%–0.40% on average).

The average Kübler Index (0.32) and the average Esquevin Index (0.26) of the AHs are approximately equal to those of the GL samples (0.33 and 0.25, respectively).

### 5.4 | Inorganic geochemistry

The major, minor and trace element concentrations determined for the GL and the AHs are available upon request. The Fe/Al ratio ranges between 0.29 and 1.16, but the average ratios of the GL and the AHs are similar (0.43 and 0.46 respectively, that is, very close to the average crustal value of McLennan, 2001). Similarly, the Ti/Al ratio, calculated to detect a hypothetical excess of aluminium compared to titanium (detrital elemental proxy; Tribouillard *et al.*, 2006), shows a constant value at 0.05 for the two groups of samples. Most importantly, the EFs of Co, Mo, U, Ba, Cu and Zn in AHs exhibit some variability (Figure 3) which can be explained by the scattered positions of samples throughout the Aptian Marnes Bleues Formation.

The redox-sensitive elements (Co, Cr, Mo, U, and V) do not show any important variation, except for Mo. Indeed, the Mo EFs of the GL are higher than those of the AHs (average EF of 3.2 and 1, respectively), with an EF up to 16 in the GL (a laminated horizon within the Sauzeries section). It is important to emphasise that 12 samples (eight in the GL, four in the AHs) were below the detection limit for Mo concentrations (1 ppm). The average EFs of U and V are slightly higher in the GL (close to 2) than those of the AHs (about 1). The average EFs of Co and Cr are the same in the two groups (close to 1). Within the GL, the redox-sensitive elements do not show enrichment (EF *ca* 1), except in the distal section of Sauzeries (Figure 3). Actually, the Mo EFs are higher (average EF of 5), and the U and V EFs are slightly higher (2.8 and 2.1 on average, respectively) than those calculated in the other sections (Figure 3).

In the same way, the productivity-sensitive elements (Ba, Cu, Ni and Zn) exhibit a monotonous distribution, the average EFs of Ba (*ca* 1), Ni (1–2) and Zn (<2) being similar for the two groups of samples. The average Cu EF is slightly higher in the AHs (3) than in the GL (*ca* 2). Within the GL, only a weak enrichment is observed in the Sauzeries sections for Ba, Cu, Ni and Zn (Figure 3).

The average IA exhibits somewhat distinct values between the AHs (3.61) and the GL (3.40). Within the GL (Figure 3), the two proximal sections, Saint-Jaume and Notre-Dame, show approximately the same average IA (3.3 and 3.27 respectively), whereas the Glaise and Sauzeries sections exhibit higher values (3.38 and 3.48, respectively).

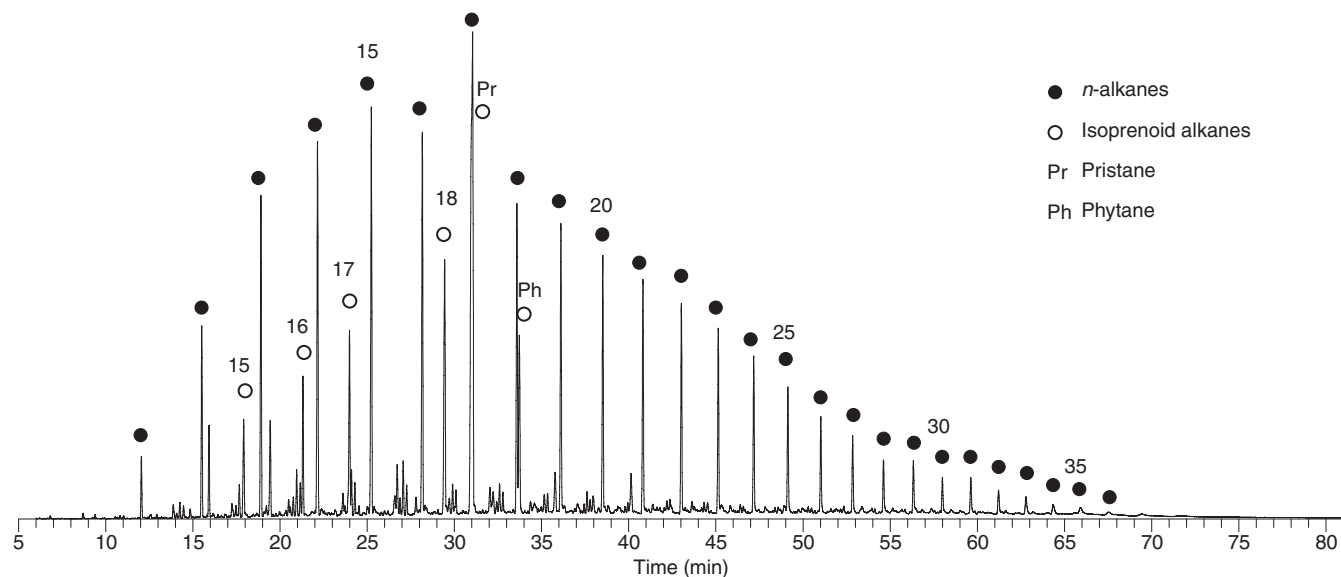


**FIGURE 5** Ion chromatogram  $m/z = 57$  showing the  $n$ -alkanes (filled dots) and the regular isoprenoids (empty dots) of the aliphatic fraction from a representative sample (SAUZ OG 005-g). Numbers above symbols denote carbon number

### 5.5 | Average SR and total organic carbon accumulation rates (TOC MARs)

Based on multiple literature references (see materials and methods), the average SRs calculated (Figure 3) were lower in the GL (0.4 to 1.5 cm/kyr) than in the AHs (3.4 cm/kyr). Moreover, the TOC MARs were the same between the AHs and the Saint-Jaume samples (44 and 46  $\text{mg cm}^{-2} \text{kyr}^{-1}$ , respectively), while the TOC MARs in the distal positions were lower (24 and 30  $\text{mg cm}^{-2} \text{kyr}^{-1}$  in the Glaise and Sauzeries sections, Figure 3).

### 5.6 | Molecular biomarkers

The  $m/z 57$  fragmentogram of the saturate fraction from a representative sample is shown in Figure 5. It shows  $n$ -alkanes ranging from  $C_{12}$  to  $C_{37}$  presenting a unimodal distribution and dominated by short chain  $n$ -alkanes with a maximum at  $C_{15}$  or  $C_{16}$ . Slight odd/even predominance is observed in  $n$ -alkanes with a carbon number higher than  $C_{23}$ . The carbon preference index (CPI) yields values between 0.67 and 1.10. The terrestrial versus aquatic ratio (TAR) presents values ranging between 0.96 and 1.35. A series of regular acyclic isoprenoids are observed in all samples. Norpristane ( $C_{18}$ ), pristane (Pr;  $C_{19}$ ) and phytane (Ph;  $C_{20}$ ) are the dominant isoprenoids (Figure 5), with Pr being the most abundant in all of the studied samples. Stratigraphic variation of the Pr/Ph ratio presents values between 1.66 and 3.85. The Pr/ $n$ - $C_{17}$  values oscillate between 0.58 and 3.15 and Ph/ $n$ - $C_{18}$  ratios between 0.37 and 1.43.

Selective ion chromatograms using  $m/z 109 + 123 + 179 + 193$  show the distribution of bicyclic sesquiterpenoids

with series ranging from  $C_{14}$  to  $C_{16}$  in all samples. Figure 6 shows peak assignments for two representative samples, where  $8\alpha(\text{H})$ - and  $8\beta(\text{H})$ -drimanes were clearly the most abundant compounds. Higher relative amounts of  $4\beta(\text{H})$ -eudesmane were also detected in samples SJ OG 006-g and ND OG 001-g while drimanes are found in higher abundance relative to eudesmane in samples from the Sauzeries section.

Hopane distributions of the analysed samples were determined based on a  $m/z 191$  ion chromatogram (Figure 7). A series of  $\alpha\beta$ -hopanes dominated by  $17\alpha(\text{H}), 21\beta(\text{H})$ -hopanes (22R and 22S epimers) were observed in all samples, showing homologues from  $C_{27}$  to  $C_{36}$  in samples from the Sauzeries and Glaise sections. In the Notre-Dame and Saint-Jaume sections, these series present homologues only until  $C_{33}$ . The proportion of  $C_{27}, C_{29}$  versus  $C_{30}$   $\alpha\beta$ -hopanes are also variable between proximal and distal sections. A series of  $\beta\alpha$ -moretanes ( $17\beta(\text{H}), 21\alpha(\text{H})$ -moretanes) were also detected ranging from  $C_{27}$  to  $C_{32}$ , with a maximum at  $C_{30}$  (Figure 7),  $C_{29}$ -hopane was present in all of the samples. Diahopanes are also present in very low amounts, especially in samples from the Sauzeries section. Two gammacerane homologs ( $C_{29}$  and  $C_{30}$ ) were also observed mostly in samples from the distal sections. Gammacerane is also observed in proximal sections but to a lesser extent and restricted to the samples SJ OG 006-g and ND OG 004-g.

Steranes and diasteranes were detected in all the samples using the characteristic fragment at  $m/z 217$  (Figure 7A,B). The proportion between regular steranes and diasteranes represented by the Dia/(Dia + Reg) ratio is almost equivalent between samples showing mean values of 0.51. Steranes are dominated by the  $C_{29}$   $5\alpha(\text{H}), 14\alpha(\text{H}), 17\alpha(\text{H})$ -20R regular

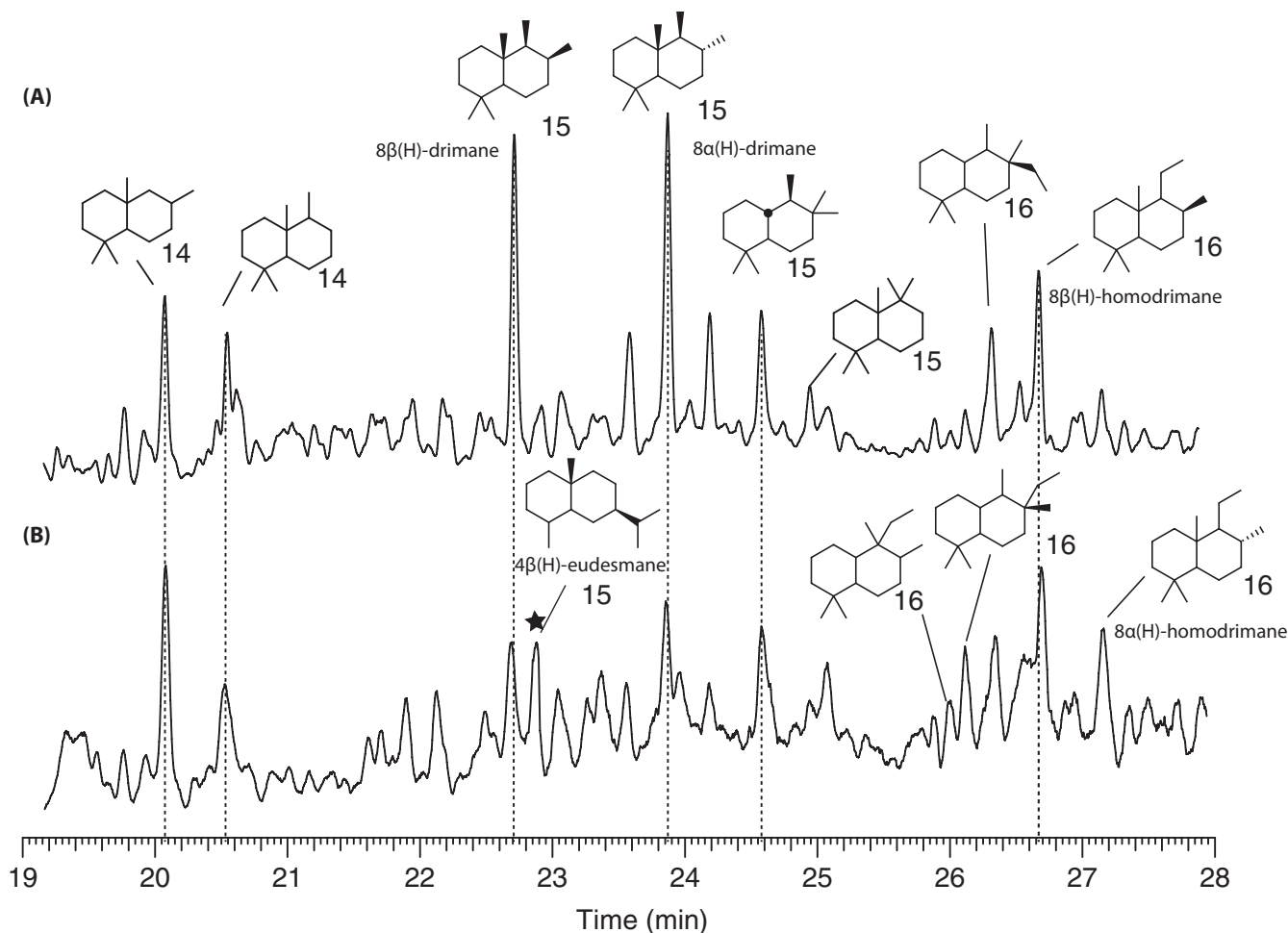


**FIGURE 6** Partial  $m/z$  109 + 123 + 179 + 193 mass fragmentograms showing the distribution of bicyclic alkanes from aliphatic fractions of two representative samples: (A) SAUZ OG 001-g; (B) ND OG 004-g. Numbers next to the structures denote carbon number. The star symbol indicates eudesmane

sterane ( $C_{29}$ -sterane; Figure 8), followed by an important contribution of the  $C_{27}$  isomer. Diasteranes are dominated by the  $C_{29}$   $\beta\alpha$ -homologue. Additionally, short chain steroids were also detected in low amounts.

Aromatic compounds are dominated by alkylnaphthalenes (methylnaphthalenes, MN; dimethylnaphthalenes, DMN; trimethylnaphthalenes, TMN), alkyphenanthrenes (phenanthrene, P; methylphenanthrenes, MP; trimethylphenanthrenes, TMP) and alkyldibenzofurans (Methyldibenzofuran, MDBF; dimethyldibenzofurans, DMDBF). Alkyldibenzofurans were detected using the ion chromatograms  $m/z$  181 + 195 + 210. The selected ion chromatograms  $m/z$  142 + 156 + 170 + 184 were used to calculate the maturity parameters from alkylnaphthalenes including the MNR, TMNr and TeMNR indices. For the alkyphenanthrenes indices (MPR, MPI1 and MPI2) the selected ion chromatograms  $m/z$  178 and 192 were used.

Monoaromatic and triaromatic steranes are also present in low amounts. Cadalene and isohexylnaphthalene are present in all samples also in trace amounts. Ion chromatogram  $m/z$

133 + 134 shows the distribution of isorenieratene derivatives (aryl-isoprenoids) in four samples (SAUZ OG 002-g, SAUZ OG 004-g, SAUZ OG 007-g and SAUZ OG 009-g) ranging from  $C_{10}$  to  $C_{25}$  (Figure 9). These compounds are absent from other sections.

## 6 | INTERPRETATIONS

Even if the GL can be characterized by several analytical techniques, it is difficult to unambiguously delineate a depositional environment for this part of the OAE 1a. In order to elaborate a depositional model for the GL in the Vocontian Basin the following points must be considered: (a) the possible impact of burial on the OM and the clay mineralogy; (b) the origin and intrinsic nature of the OM; (c) the impact of the SRs on the organic content; (d) the oxygenation conditions during the deposition of the GL; and (e) surface-water productivity during the OAE 1a in the Vocontian Basin.

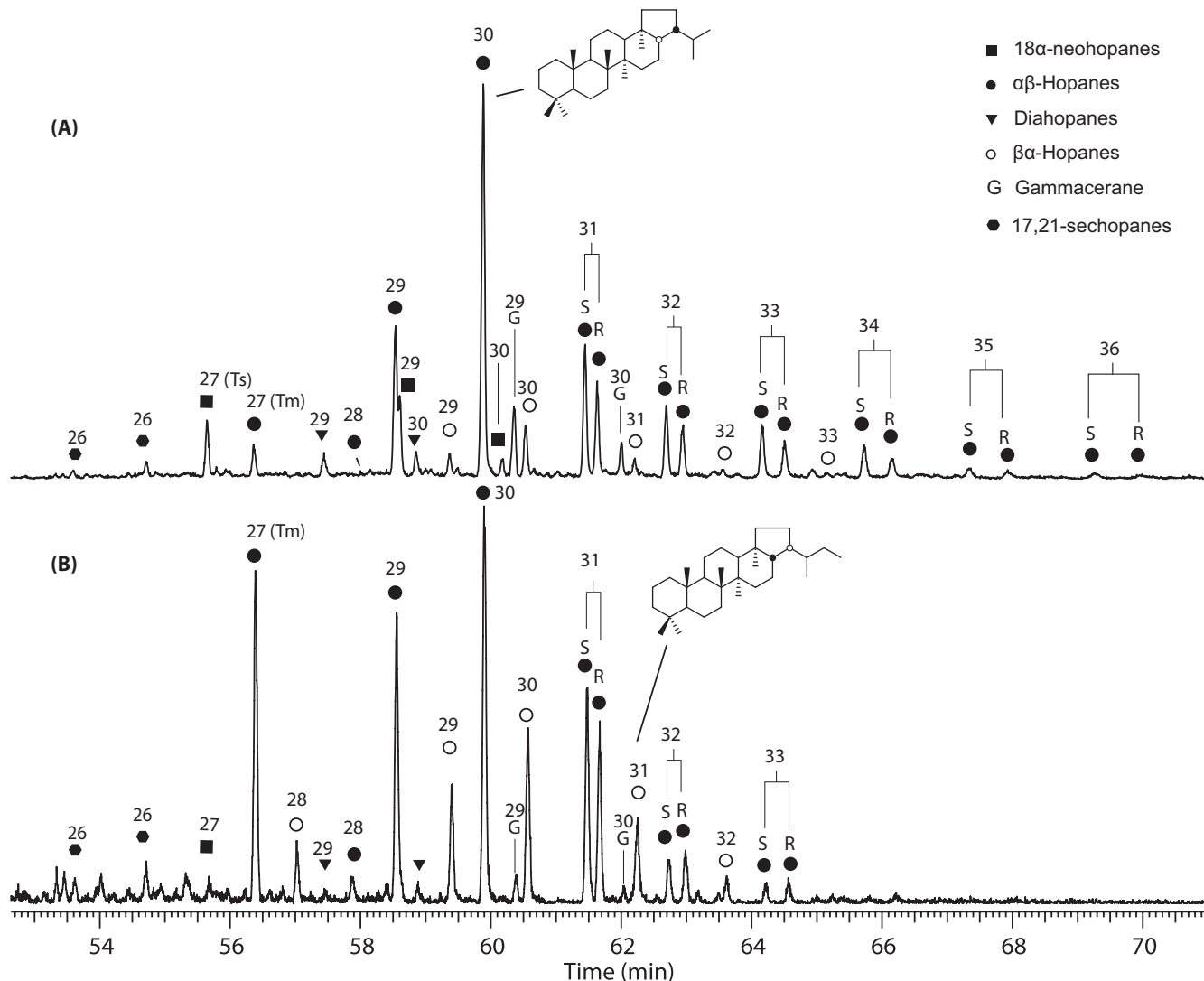


**FIGURE 7** Representative fragmentograms ( $m/z = 191$ ) showing the hopanoid distribution of two samples: (A) SAUZ OG 005-g; (B) SJ OG 006-g from the Goguel Level

## 6.1 | Impact of burial

From the Rock-Eval data, the OM of the Marnes Bleues Formation shows low maturity (immature stage to onset of oil window in a HI-Tmax diagram, Figure 4), and the molecular biomarkers support this. The distribution patterns of alkylnaphthalenes are dominated by low-maturity isomers, for example, 1,2,5,6-1,2,3,5-tetramethylnaphthalenes (TeMN) over 1,3,6,7-TeMN, showing ratios of  $<1$  (van Aarssen *et al.*, 1999). Alkylphenanthrenes also show a similar trend, with a distribution dominated by 9-methylphenanthrene over 1-methylphenanthrene (e.g. MPI1  $< 1$ ; Radke *et al.*, 1986). Other biomarkers indicative of low maturity include the contribution of low-maturity hopane homologues ( $\beta\alpha$ -moretanes; Peters *et al.*, 2005; and references therein), the absence, or low abundance, of the high-maturity  $C_{27}$  hopane homologue (Ts: 18 $\alpha$ -22,29,30-trisnorhopane; Figure 7) and the relatively

low abundance of  $\alpha\beta$ -steranes over  $\beta\alpha$ -sterane homologues (Figure 9; Seifert and Michael Moldowan, 1978).

The clay assemblages show a decrease (Glaise section) and a lack (Sauzeries section) of smectite in distal locations. Such variations suggest possible illitization of smectite into I-S during diagenesis. To test this hypothesis, a diagram of the Esquevin Index versus the Kübler Index (Kübler, 1967; Esquevin, 1969; Dunoyer de Seconzac, 1969; Kübler and Jaboyedoff, 2000) can be used to compare the burial of various sections (Figure 10). In this diagram, all samples (AHs and GL) fall into the 'anchizone' for the Kübler Index and into the 'biotite + muscovite' zone for the Esquevin Index, indicating similar burial effects on all sections. However, the 'anchizone' deduced from illite crystallinity involves a higher burial than the OM results show. Thus, two possibilities can be envisaged for the illite origin: (a) neoformation of sediments during significant burial or (b) a detrital origin, with prior burial within

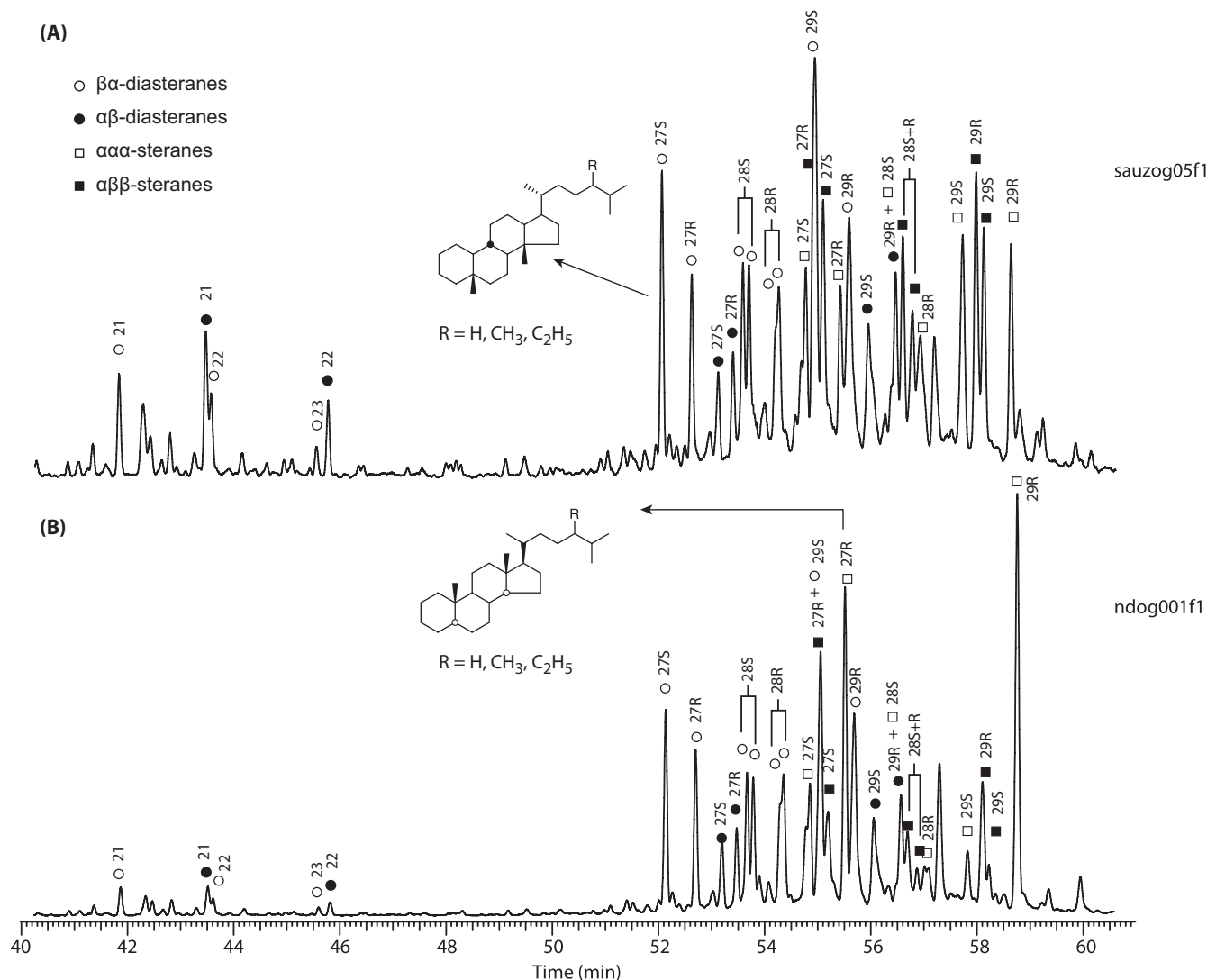


**FIGURE 8** Representative fragmentograms ( $m/z = 217$ ) showing the steroid distribution of two samples: (A) SAUZ OG 005-g; (B) ND OG 001-g from the Goguel Level

another geological formation (Kübler and Jaboyedoff, 2000). If the smectite had been transformed into I-S during diagenesis, the I-S/illite ratio (the two major components of the clay assemblages in the GL) would show increased burial for the distal sections, compared to the proximal sections. In fact, the average ratios of I-S/illite are relatively similar: 1.0 in the Notre-Dame section; 1.7 in the Saint-Jaume section; 1.7 in the Glaise section; and 1.5 in the Sauzeries section. Thus, there is no major variation in I-S in the clay assemblages that could be interpreted as the illitization of smectite minerals. The loss of smectite could be explained by contrasting clay source areas discriminating between proximal and distal sections. In addition, the discrimination of clay-mineral source areas is consistent with the values of IA that differentiate proximal and distal sections. Another explanation (or a complementary one) is that a proportion of the smectite could have been transformed into chlorite during diagenesis (Tribovillard, 1989), which is

consistent with the high proportion of chlorite in the Sauzeries section (17% on average). These observations suggest a detrital origin for the illite in the Vocontian Basin during the Aptian.

Thus, except for the smectite variations in the distal sections, the clay minerals can be interpreted as being sedimentary signatures of what the emerged lands supplied to the basin. The weak imprint of diagenesis on the clay assemblages is consistent with previous studies (Deconinck, 1984; 1987; Levert and Ferry, 1988; Ghirardi *et al.*, 2014); however, diagenesis could have locally impacted the clay assemblages and the OM in the localities close to the Alpine Thrust Front in the eastern part of the Vocontian Basin (Levert and Ferry, 1988). From examination of the clay assemblages (Levert and Ferry, 1987), the maximum burial depth in the western part of the basin was estimated to range between 500 and 1,000 m.

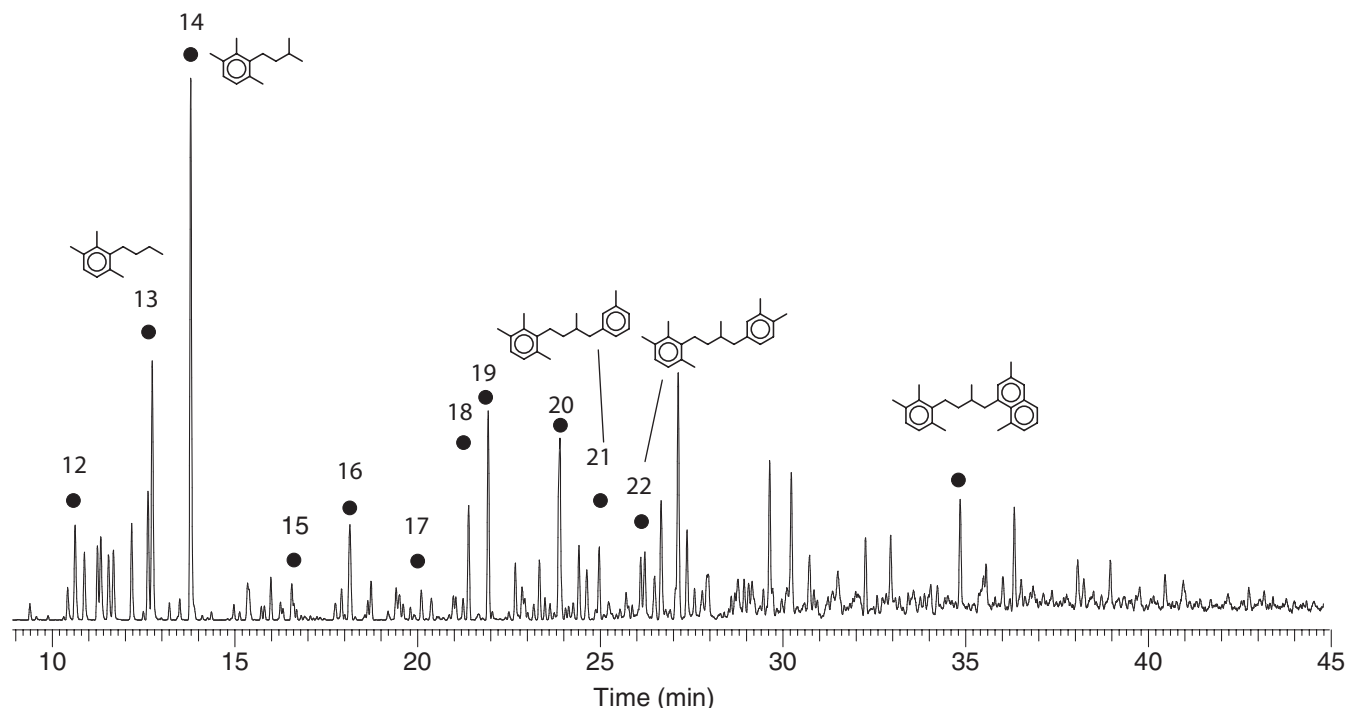


**FIGURE 9** Partial ion chromatogram  $m/z$  133 + 134 showing the distribution of aryl isoprenoids present in the studied extracts

## 6.2 | Nature of the OM

The origin of the OM was determined by comparing the four studied sections in terms of the Rock-Eval parameters (TOC, HI,  $T_{max}$ ) and biomarker assemblages. Rock-Eval parameters show variable HI values (66–520 mgHC/gTOC), covering the fields of type-II and type-III kerogens. More conspicuously, a  $T_{max}$  versus HI crossplot (Figure 4) shows that the hemipelagite samples (that is, the background sedimentation) plot within the Type-III area whereas most of the Goguel samples are scattered throughout the Type-II area, with the Sauzerie section samples yielding the highest HI values.

The information retrieved from the aliphatic linear biomarkers show a distribution of  $n$ -alkanes that may be indicative of the OM source. The proportion of algal-derived versus land plant-derived  $n$ -alkanes is commonly used to corroborate the origin of OM. For instance, algal-bacterial OM is rich in short-chain  $n$ -alkanes ( $<C_{20}$ ), and land plant-derived OM is dominated by long-chain  $n$ -alkanes ( $>C_{27}$ ) showing an odd-over-even carbon number predominance (OEP; Eglinton and Hamilton, 1967; Cranwell *et al.*, 1987). One of the ratios commonly employed to numerically represent the OEP is the CPI. In the studied samples, the CPI shows two main values: (a) sections with average values of *ca* 1 (Glaise: mean CPI = 1.03; Sauzeries: mean CPI = 0.94); and (b) samples with average values of  $<1$  (Notre-Dame: mean CPI = 0.74; Saint-Jaume: mean CPI = 0.81). These results are consistent with the TAR ratio showing higher values in the most proximal

sequences. The values suggest a marine OM source, with a higher land plant influence, in the Notre-Dame and Saint-Jaume sections.

Bicyclic sesquiterpenoids can also be indicative of the type of OM input. Eudesmane derivatives are land plant biomarkers commonly attributed to angiosperms, gymnosperms (Noble, 1986; Ahmed *et al.*, 1990) and liverworts (Liu *et al.*, 2012). The sediments studied show a gradient in the relative concentrations of these bicyclic compounds. The highest relative amounts are observed in the Saint-Jaume and Notre-Dame sections. The distal sections contain relatively low amounts of eudesmane-type compounds (Figure 6). The same trend is observed in land-derived aromatic compounds from the sediment extracts, which show a higher input in the proximal sections. For instance, the aromatic fractions of the proximal sections show higher inputs of methylated dibenzofuran derivatives (MDBF/MN), which are the major products of land plant-derived kerogens, coals (Stefanova *et al.*, 1995; Radke *et al.*, 2000; Romero-Sarmiento *et al.*, 2011) and primitive thaloids (Quijada *et al.*, 2015). These derive from the polycondensation of lignin and lignin degradation products (Hatcher and Clifford, 1997), but they are also accepted as thermal degradation products of cellulose (Pastorova *et al.*, 1994).

The sterane distribution, dominated by  $C_{29}$  and  $C_{27}$  isomers, is typical of marine algal OM. Other algal biomarkers, including methylated steroids, and in particular 4-methyl steroids, which are often assigned to dinoflagellates (dinosteroid) and/or acritarchs, are absent or present in low amounts. The presence of high amounts of

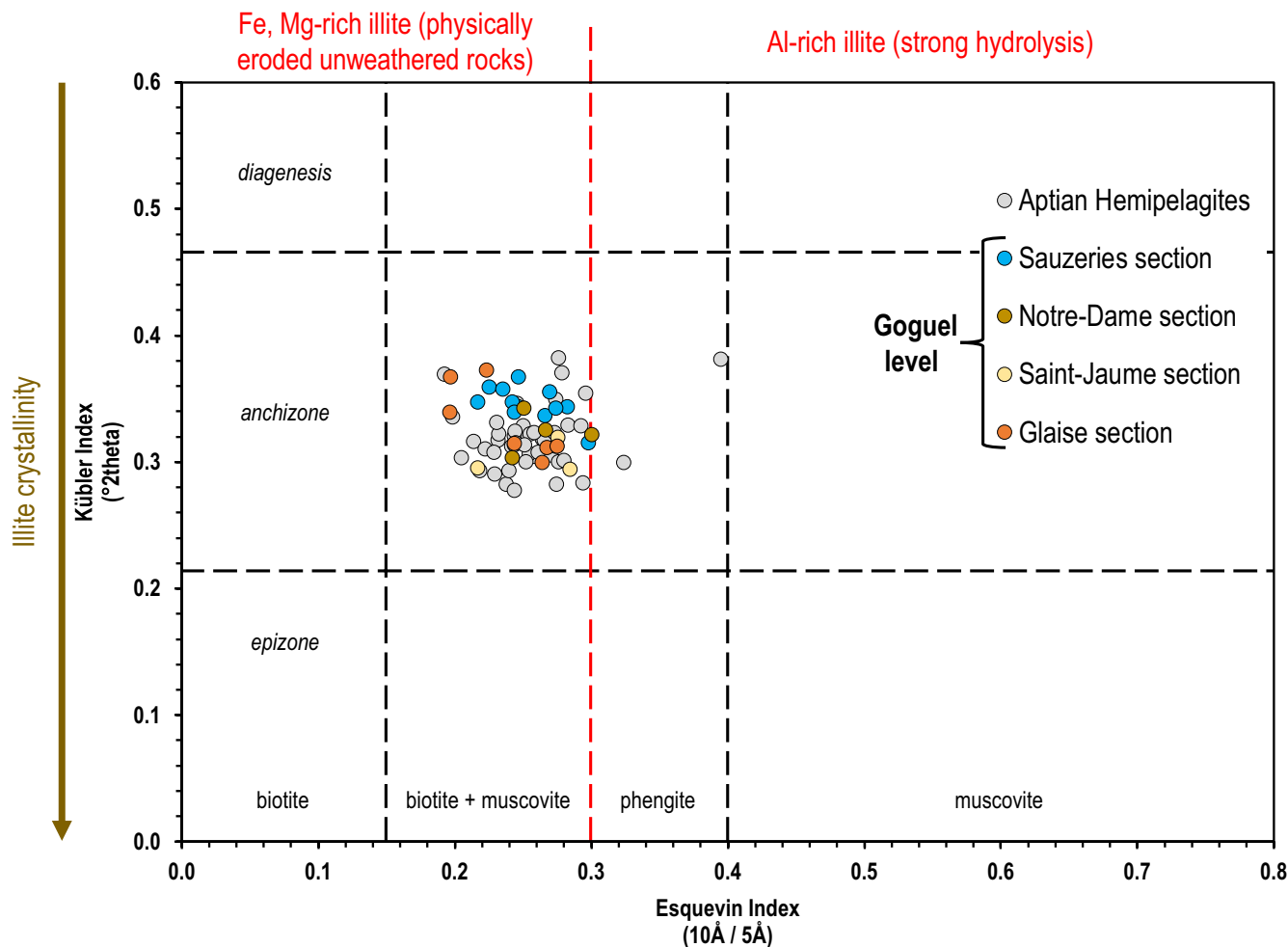


**FIGURE 10** Plot of Esquevin Index versus Kübler Index indicating the burial from the clay minerals of the studied samples (diagram from Kübler, 1967; Dunoyer de Seconzac, 1969; Esquevin, 1969; Kübler and Jaboyedoff, 2000)

pentacyclic terpenoids, with hopanoid skeletons and their diagenesis products, attest to a bacterial contribution. This is corroborated by the presence of bicyclic sesquiterpenoids, including drimane and homodrimane homologues (Ourisson *et al.*, 1979; Alexander *et al.*, 1987). The hopane/sterane ratio is often used to compare the relative proportion of eukaryotic versus bacterial biomass. The lowest values of this ratio are observed in the samples from the proximal sections, suggesting a higher contribution from eukaryotes in these samples, while a higher contribution from bacterial biomass is observed in the distal sections.

On the basis of the molecular biomarker results, two groups of OM are determined: (a) the ‘proximal’ OM deposited in an upper slope environment (Saint-Jaume and Notre-Dame sections), which has a higher contribution from terrestrial OM and eukaryotes (for the marine OM contribution) and (b) the ‘distal’ pattern of OM, as recorded in the lower slope locations (Glaise and Sauzeries sections), which has a higher contribution of marine OM derived from bacterial biomass.

### 6.3 | Dilution versus the condensation of OM

According to previous studies (Bréhéret, 1997; Heimhofer *et al.*, 2006), the GL has been interpreted as an interval of condensation, particularly when comparing it to the background sedimentation of the Marnes Bleues Formation. Indeed, the average SRs of the GL were at least three times lower than the AHs (Figure 3); however, a comparison of the average SRs of three of the sections (Saint-Jaume, Glaise and Sauzeries) allows a determination of the role of condensation in the OM sedimentation in the GL. In fact, the only OM-rich section (Sauzeries) shows a very low average SR (0.4 cm/kyr). Moreover, the comparable TOC MARs in the two distal sections (Glaise and Sauzeries, Figure 3) indicate that the OM enrichment cannot be explained by a higher input of OM in this part of the basin.

Similarly, variations in carbonate content in the GL can also be explained in terms of dilution and condensation. The carbonate fraction was less diluted in the Sauzeries section than in the other sections, because its dilution/condensation

was the direct consequence of detrital input, as proposed by Br  h  ret (1997).

## 6.4 | Oxygenation in the depositional environments

The general trend of the trace element distribution indicates that the Vocontian Basin was homogeneous regarding redox conditions during the OAE 1a, contrary to the organic proxies (molecular biomarkers).

Herein, several lipid biomarker proxies are used to assess potential differences in oxygenation. The first is gammacerane, a saturated compound derived from the de-functionalization of tetrahymanol, that is, a compound biosynthesized by bacteriophage ciliates living at the thermocline in stratified water-columns (Ten Haven *et al.*, 1989; Harvey and McManus, 1991; Sinninghe Damst   *et al.*, 1995). Accordingly, the moderate to low abundances of gammacerane derivatives observed in the samples from the GL can be used to probe the presence of a water-column stratification that was formed by a difference in temperature or salinity. The highest relative concentrations of gammacerane homologues are observed in the distal section of Sauzeries. Nevertheless, these compounds are not present along the entire studied interval, suggesting the intermittent appearance of water-column stratification and the onset of relatively more reducing conditions in the deep basin.

Consistent with the detection of gammacerane, the hopane/sterane ratio shows higher values in the distal sections. The hopane/sterane ratio is also used as an indirect proxy for oxygenation conditions during OM deposition. Hopanoids are exclusively produced by bacteria (Ourisson *et al.*, 1979). Recent discussions about hopanoid provenance indicate that the enhanced production of hopanoids has been observed in association with suboxic and anoxic depths within a chemocline in stratified water-columns (Blumenberg *et al.*, 2010; S  enz *et al.*, 2011; Rohrsen *et al.*, 2013). Accordingly, the occurrence of higher inputs of hopanoids versus steranes in distal sections could be associated with the presence of a hypoxic zone in the upper part of the water-column in the distal part of the basin, derived from OM remineralization and consequent oxygen consumption. Concomitant with these proxies, the detection of aryl isoprenoids in the samples from the Sauzeries section indicates sporadic periods of hypoxia. These compounds derive from isorenieratene, which is an aromatic carotenoid synthesized by green (Chlorobiaceae) and purple sulphur bacteria (Chromatiaceae) (Schaeffer *et al.*, 1997; Clifford *et al.*, 1998; Brocks and Schaeffer, 2008), which are photosynthetic anaerobic organisms that require reduced sulphur to live. Thus, isorenieratene derivatives are widely used as proxies for photic zone euxinia during OM

deposition (Koopmans *et al.*, 1996; Sinninghe Damst   and Koopmans, 1997; Schaeffer *et al.*, 1997; J  nior *et al.*, 2013; Quijada *et al.*, 2015). The use of aryl isoprenoids as proxies for water-column euxinia has to be handled carefully since these compounds can also derive from the aromatization of  $\beta$ -carotane (Koopmans *et al.*, 1996). Nevertheless, the presence of these compounds alongside the other parameters of water-column stratification and hypoxia in the distal GL samples, may reflect the initial productivity of Chlorobiaceae. In fact, the relatively limited preservation of intermediate-chain derivatives implies that euxinic conditions were not persistent (Schwark and Frimmel, 2004), reflecting intermittently stable water-column stratification. The occurrence of water-column stratification, and subsequent hypoxia in the water-column, is consistent with previous data reported for the ‘Selli Level’ in Italy, based on molecular biomarkers and palynomorphs (Heimhofer *et al.*, 2004; Pancost *et al.*, 2004; van Breugel *et al.*, 2007).

According to the redox-sensitive elements, depositional conditions during the GL were approximately similar to the background sedimentation of the entire Marnes Bleues Formation—that is, relatively oxygenated. The great variability in the redox and productivity EFs of the AHs can be explained by the scattered positions of the samples in the Marnes Bleues Formation because the depositional conditions somewhat fluctuated during the Aptian, which lasted several million years.

The exception is the Sauzeries section, in which Mo, U and V-EFs are moderately enriched (Figure 3). According to Tribovillard *et al.* (2012), a U-EF versus Mo-EF crossplot allows the redox conditions during deposition of the GL to be determined (Figure 11). Herein, the Mo and U distributions indicate suboxic to anoxic conditions during deposition of the GL in the Sauzeries section, and oxic conditions in all the other sections, including the (distal) Glaise section.

Although the sampling protocol employed here smoothed the geochemical signal (each sample being several centimetres thick, so covering several thousand years of deposition), it is surprising to observe low to moderate EFs for selected redox-sensitive elements. Two possible mechanisms may account for these results: (a) the ‘basin reservoir effect’ (Algeo and Lyons, 2006; Algeo and Tribovillard, 2009) and (b) the ‘burn-down effect’ (Middleburg and De Lange, 1988; Prah *et al.*, 2003).

1. The ‘basin reservoir effect’ would be linked to the position of the Vocontian Basin in the Tethys Ocean. The connection between the basin and the ocean was achieved through a relatively narrow seaway (Figure 1), which could have resulted in limited renewal of bottom waters (Br  h  ret, 1997). The oceanic circulation patterns reconstructed for the Vocontian Basin indicate east-to-west

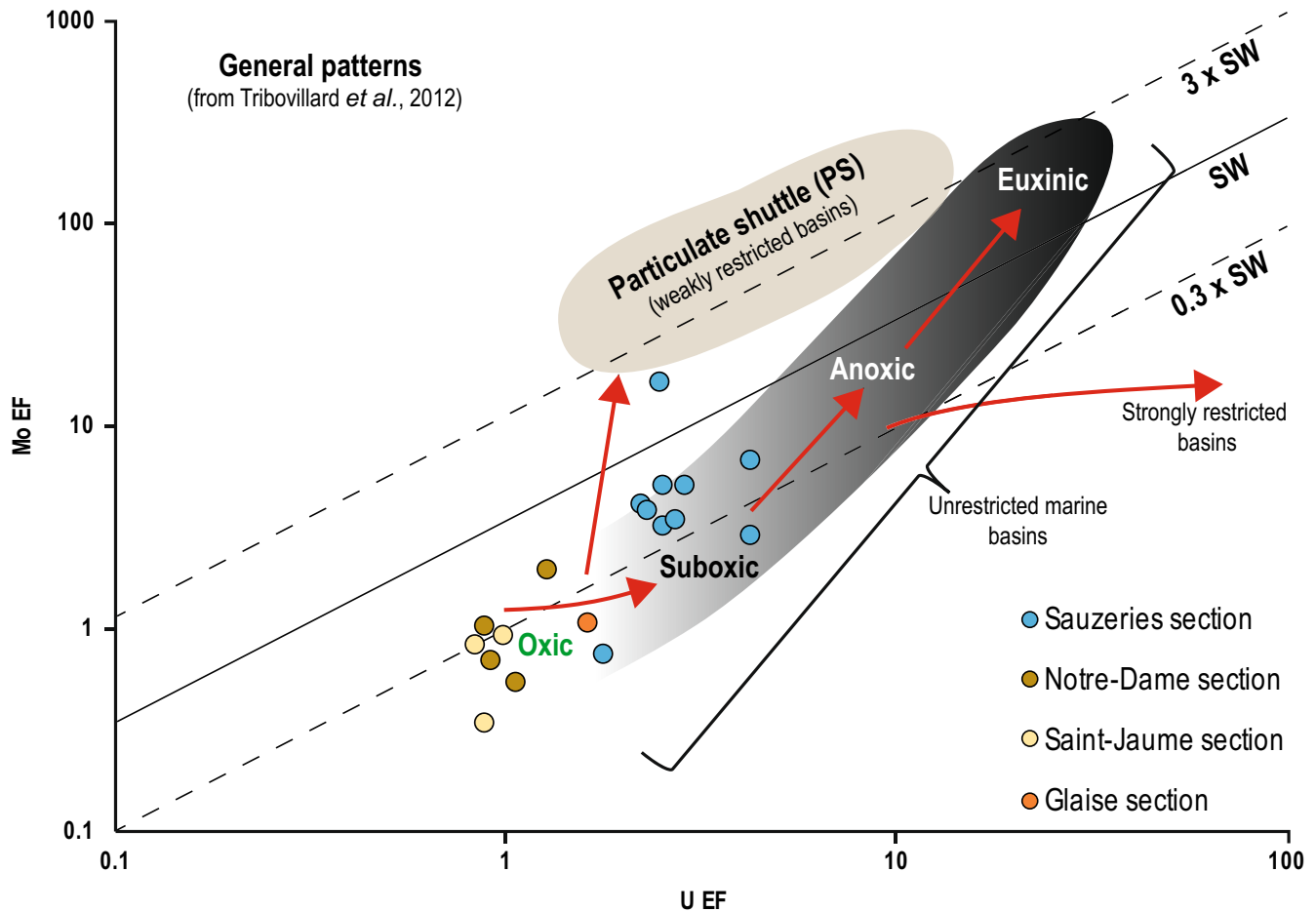


**FIGURE 11** Plot of U-EF versus Mo-EF for the GL samples showing the oxygenation conditions in the Goguel Level. The SW lines corresponds to the Mo/U molar ratios similar to the seawater value (SW ~7.5 to 7.9) and the dashed lines correspond to the fractions thereof ( $3 \times \text{SW}$ ,  $0.3 \times \text{SW}$ ). The pattern of U and Mo EFs are compared to the model proposed in Algeo and Tribovillard (2009)

currents along the northern coast of the basin (Delamette, 1990; Föllmi *et al.*, 2011). Moreover, in other parts of the Tethys Ocean, the OAE 1a is classically associated with poorly oxygenated bottom waters, as evidenced by the widespread deposition of black shales, and with strong enrichments in redox-sensitive elements (Stein *et al.*, 2011; Föllmi *et al.*, 2012; Westermann *et al.*, 2013; Khaled *et al.*, 2017). Consequently, the waters pushed into the Vocontian Basin via this narrow seaway could have originally been (partly) depleted in redox-sensitive elements through the so-called ‘basin reservoir effect’ (Algeo and Lyons, 2006; Algeo and Tribovillard, 2009), and the limited renewal of deep-waters could have further enhanced the initial depletion in dissolved, redox-sensitive elements in the Vocontian Basin water-mass. In the same way, the limited renewal of deep-waters may have caused (intermittent?) water-column stratification.

2. The ‘burn-down effect’ could have impacted redox-sensitive element concentrations in the sediments via oxygenation and post-depositional re-oxygenation by turbiditic deposits in the sections containing abundant

turbidites (Saint-Jaume, Notre-Dame and Glaise). The recurrent input of turbiditic currents may have oxygenated the deep-water mass of the basin for very brief periods, and, in particular, could have re-oxygenated the sediment-water interface and, in turn, the underlying sediments, as observed in the Madeira Abyssal Plain (Thomson *et al.*, 1984; Middleburg and De Lange, 1988; Prahl *et al.*, 2003). In addition, these recurrent turbiditic currents could have locally disrupted the water-column stratification for very short episodes, particularly in the proximal sections where gammacerane abundances are very low.

## 6.5 | Role of productivity

Herein, the productivity-sensitive elements show EFs close to 1 in all sections; the absence of authigenic enrichment strongly suggests that productivity remained at a low level (i.e. low or normal levels of productivity). Moreover, the TOC MARs are relatively similar in the distal sections (Glaise and Sauzeries), and weakly higher in the proximal

section (Saint-Jaume). The Sauzeries section contains the highest OM abundance and, if productivity had been strong during GL deposition, the TOC MARs would have been distinctly higher there than in the other sections, and in the AHs. In addition to these results, the clay assemblages and the IA provide some indications of the low to normal primary productivity in the basin. There is no increase in either kaolinite (a clay mineral formed under strongly hydrolysing conditions, supplying nutrients to the marine waters; Chamley, 1989) or IA (the index related to chemical hydrolysis of emerged lands, Von Eynatten *et al.*, 2003) relative to the background sedimentation of the Marnes Bleues Formation. These two observations, derived from a limited fraction of the sediment (clay minerals), and from the bulk detrital fraction of the sediment (IA), suggest that no marked climate change occurred during the GL deposition in the Vocontian Basin drainage area. Finally, the absence of major climate change in the sedimentary source areas, as previously proposed by Br  h  ret (1997) and Heimhofer *et al.* (2004), is fully consistent with the low to normal surface-water productivity inferred from the trace element distributions. In conclusion, it is believed that: (a) surface-water productivity was not a major cause of enrichment in OM in the GL and (b) periodic water-column stratification, demonstrated by molecular biomarkers, was not triggered by the productivity-driven model or by an increase in continental freshwater input.

## 7 | DISCUSSION: IMPACT OF SEDIMENTARY CONDENSATION AND TURBIDITE INPUT INTO THE DEEP PART OF A POORLY-OXYGENATED BASIN

### 7.1 | Depositional model for the GL in the Vocontian Basin during the OAE 1a

Primarily, the main difference between the studied four sections that contain the GL is the occurrence/absence of turbidites. Thus, the input of detrital materials, via turbiditic currents, have induced the dilution of OM in the GL. In addition, the results suggest (intermittent) water-column stratification with: (a) hypoxia in the photic-zone surface water, which was more marked in the distal sections (molecular biomarkers) and (b) suboxic to anoxic conditions in the lower slope environment (molecular biomarkers and inorganic geochemistry). Due to the limited renewal of deep waters in the Vocontian Basin (Br  h  ret, 1997), the deep basin was ill-ventilated. Consequently, to account for the absence of redox-sensitive trace elements, the proposed model highlights the re-oxygenation of the bottom waters by turbiditic currents that triggered the long-term ‘burn-down effect’ (Figure 12).

Over the upper slope (Saint-Jaume and Notre-Dame sections), as indicated by the organic compounds and the inorganic geochemistry, the depositional conditions were relatively well oxygenated, and productivity was low to normal. The proximity of terrigenous source areas is suggested by the relatively high contributions of terrestrial OM to the biomarker distribution. The input of detrital material (via numerous turbidites) is observed in tandem with sand enriched sediments and relatively high calculated SRs; these could also have disrupted water-column stratification (Figure 12). It is proposed here that the low organic content in the GL was a consequence of the dilution (by detrital input) and destruction (under oxic conditions) of OM during deposition of the sediments. In addition, the low carbonate content could be interpreted as reflecting low productivity and relatively high clastic supply. The relatively high TOC MARs in the Saint-Jaume section, compared to the distal sections, was probably due to the abundance of land-derived, refractory, ‘proximal’ OM, which was richer in terrigenous products, compared to ‘distal’ OM.

Over the lower slope (Glaise and Sauzeries sections), the OM signature is also specific. The molecular biomarkers here denote the relatively strong contribution of marine OM (algal-bacterial), in contrast to the proximal sections. The low proportion of sands in the clastic fraction also confirms the distal position. The molecular markers suggest strong water-column stratification, in particular in the Sauzeries section (confirmed by the inorganic geochemistry), and the productivity was again low to normal. However, the organic content, the inorganic geochemistry and the average SRs calculated differ between both deeper sections. Based on these arguments, the roles of dilution and remineralization (oxygenation) can be considered. Indeed, the ‘distal’ OM deposited in the Glaise section indicates water-column stratification at the molecular scale, but the numerous turbidites probably diluted and destroyed (post-depositional re-oxidation through the ‘burn-down effect’) most of the OM during deposition of the sediments. In addition to dilution of sediment OM, the turbidite currents could have oxygenated the bottom waters (destructive effect) and re-oxygenated the underlying sediments (‘burn-down effect’). Similar to what is observed in the proximal sections, the low carbonate content could be the result of this dilution effect by detrital material. In the Sauzeries section, the environmental conditions were the opposite. The organic compounds and the inorganic geochemistry (Figure 7) clearly indicate strong water-column stratification, coupled with deep suboxic to anoxic conditions, during a period of condensation (very low average SR). Based on the observations reported here, the depositional model suggests condensed sedimentation in a low-oxygen environment, expressed by the concentration and preservation of OM. The relatively low TOC MARs in the distal sections show that the productivity was no higher

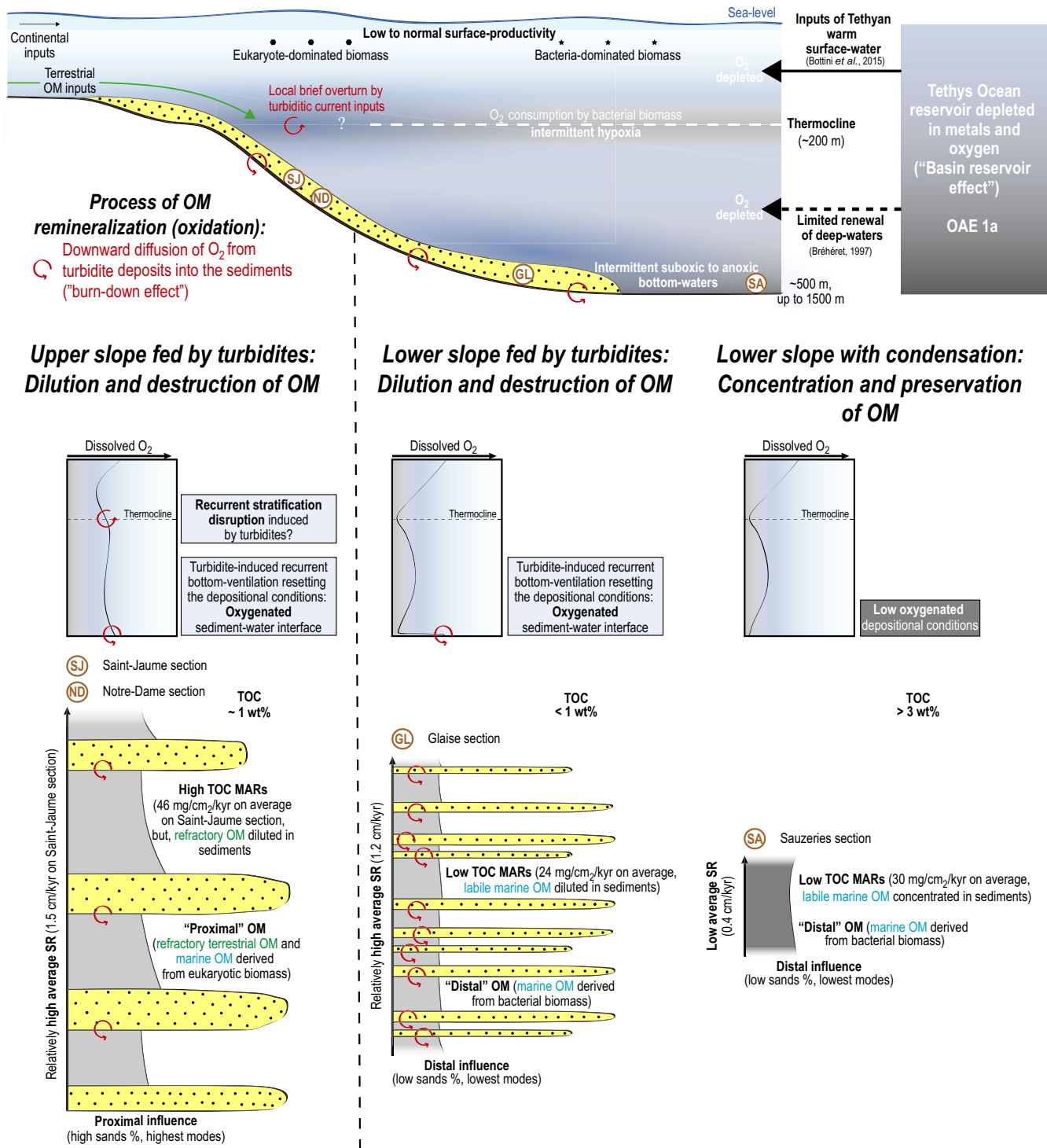


**FIGURE 12** Model of organic matter sedimentation along the margin of the Vocontian Basin during the OAE 1a. Section locations are reported in Figure 1

there than in the upper slope environment, and that the very low values in the Glaise section can be explained by degradation of the more labile algal-bacterial OM under oxygenated conditions.

The study of four sections on the slope of the Vocontian Basin allows a depositional model to be built that includes

water-column stratification during the GL (Figure 12), with three specific environments identified impacting OM sedimentation: (a) the upper slope environment, fed by turbidites, with dilution (induced by turbidites) and destruction of ‘proximal’ (i.e. terrestrial-dominated) OM under oxic conditions (possible disruption of water-column stratification by

turbiditic overturn); (b) the lower slope environment, initially weakly oxygenated, fed by turbidites, with dilution and destruction of ‘distal’ (i.e. marine-dominated) OM, both process probably induced by turbidites; and (c) the lower slope environment without turbidites, with sedimentary condensation in a low-oxygenation context, where the concentration and preservation of specific ‘distal’ OM was substantially furthered.

## 7.2 | Impact of dilution on organic contents

The OM distribution in the GL highlights the role of low SRs coupled with low oxygenation in a stratified deep basin. In fact, based on numerous modern and ancient examples, these conditions have been described as the best way to attain OM enrichment in sediments (Stein *et al.*, 1986; Creaney and Passey, 1993; Tyson, 2001, 2005; Sageman *et al.*, 2003; Bohacs *et al.*, 2005). Actually, increased accumulation of carbonate and clastic materials dilutes organic carbon in sediments. According to Tyson (2001, 2005), the highest OM enrichment occurs in condensed sections (<1 to 5 cm/kyr) under dysoxic-anoxic conditions. Although comparing calculated average SRs with other data must be done cautiously (see subSection 4.6), it has been shown herein that the average SR of the Sauzeries section was in the range of the SRs proposed by Tyson (2001, 2005).

## 7.3 | OM remineralization by the ‘burn-down effect’

The oxygen regime was the other major criterion highlighted in the depositional model proposed for the GL. In the Sauzeries section, the redox-sensitive elements indicate low oxygenation, but in the other sections, the GL was clearly deposited under oxic conditions. Although the ‘basin reservoir effect’ (Algeo and Lyons, 2006; Algeo and Tribovillard, 2009) may have impacted the inorganic geochemistry, the periodic flows of turbidites must have oxygenated the bottom waters and, especially, the sediment-water interface and underlying sediments (Rubino, 1989). Moreover, in the well-described example of the Madeira Abyssal Plain (Middleburg and De Lange, 1988; Cowie *et al.*, 1995; Prah *et al.*, 1997, 2003; Thomson *et al.*, 1998; Hoefs *et al.*, 2002) and the Iberia Abyssal Plain (Meyers *et al.*, 1996), the ‘burn-down effect’ (Thomson *et al.*, 1984; Middleburg and De Lange, 1988; Prah *et al.*, 2003) corresponds to the post-depositional remineralization of OM. In detail, the low SRs of the hemipelagic deposits, coupled with frequent turbiditic input, resulted in the early diagenetic re-oxidation of OM in the underlying sediments by downward oxygen diffusion. In the sediments capped by thin turbidite deposits, the ‘burn-down

effect’ was deduced from the decrease in several trace element abundances and from biomarker evidences up to *ca* 15 cm below the sediment-water interface in recent sediments (Cowie *et al.*, 1995; Prah *et al.*, 1997, 2003; Thomson *et al.*, 1998; Hoefs *et al.*, 2002). On the other hand, the high SRs in hemipelagic sediments associated with thick turbiditic beds quickly seal the underlying sediments and further the depletion of oxygen and the sulphate reduction-related destruction of OM (Meyers *et al.*, 1996). Even if the present study does not take compaction into consideration, the calculated average SRs for the sections with thin turbidites (1.5 and 1.2 cm/kyr in the Saint-Jaume and Glaise sections, respectively) were three times less than the average SR in the Marnes Bleues Formation (3.4 cm/kyr) and, thereby, the average SRs corresponding to the GL interbedded with thin turbidites (millimetres to multiples of centimetres thick, Rubino, 1989; Friès and Parize, 2003) can be considered to be low in the Vocontian Basin. In addition, the numerous thin turbiditic deposits observed in the sections are vertically stacked, with a *ca* 10 cm step, implying that the recurrence of turbiditic currents, and therefore of oxygen inputs to the sediment-water interface, was sufficient to maintain an efficient long-term ‘burn-down effect’ within the GL sediments.

Consequently, it is proposed that the slow SRs associated with brief, recurrent, turbiditic inputs degraded the original OM in the sediments of the GL via oxygen export to the sediment-water interface at the bottom of the Vocontian Basin, triggering long-term post-depositional re-oxygenation of the underlying organic carbon (Figure 12). In addition, if the interval between two successive turbidites was less than the thickness of sediment involved in the ‘burn down effect’, this may account for the depositional redox record being post-depositionally erased or ‘bleached’, erroneously suggesting normal marine conditions of deposition in the parts of the basin influenced by recurrent re-sedimentation.

## 7.4 | Origin of the water-column stratification in the Vocontian Basin

In the ‘classical’ model, an increase in primary productivity has been thought to have triggered the depletion of oxygen at the bottom of the ocean at the onset of the OAE 1a (Weissert, 1990; Föllmi, 1995; Sanfourche and Baudin, 2001; Westermann *et al.*, 2013). In addition, Westermann *et al.* (2013) proposed that changes in the oxygenation conditions in the Tethys Ocean were associated with a fluctuating oxygen minimum zone, induced by high primary productivity, rather than stronger ocean stratification. With dilution and oxygenation being key factors in the present study, the role of primary productivity can be challenged (Heimhofer *et al.*, 2006; this study). The conclusions of Westermann *et al.* (2013) were mainly deduced from the

Gorgo a Cerbara section in central Italy, which corresponded to the deep Tethys Ocean during the OAE 1a. In the Glaise section, the organic content and inorganic geochemistry results are in the same range as those from this study (figs 2 and 4B in Westermann *et al.*, 2013). According to results in the Vocontian Basin (Westermann *et al.*, 2013; this study), the surface-water productivity was low to normal.

Nevertheless, the ‘classical’ model of the OAE 1a is not inconsistent with the results in the Vocontian Basin. In this stratified basin, two depleted oxygen minimum zones were (episodically) present: in the photic zone and the deep basin (Figure 12). It is proposed here that the waters pushed into the Vocontian Basin had been previously depleted in oxygen in the Tethys Ocean by high primary productivity, as proposed in the ‘classical’ model for the OAE 1a. As previously discussed in relation to the ‘basin reservoir effect’ (Section 6.4), the Vocontian Basin was a diverticulum of the Tethys Ocean in which only limited renewal of the bottom waters occurred (Bréhéret, 1997), favouring water-column stratification. Moreover, the surface-water palaeotemperatures calculated for the Aptian in the Tethys Ocean were high (Bottini *et al.*, 2015), and the solubility of atmospheric oxygen decreases with the warming of surface waters (Weiss, 1970). Therefore, the water-column stratification observed in the Vocontian Basin could have been caused by: (a) the input of depleted-oxygen waters from the Tethys Ocean (caused by OAE 1a-related high productivity); (b) the limited connection with the Tethys Ocean; and (c) the relatively warm surface waters.

### 7.5 | Hypothetical impact of palaeogeography on the clay mineralogy

During the Lower Cretaceous, tectonic subsidence was more pronounced in the eastern part of the Vocontian Basin than in the south-eastern part, which explains the occurrence of numerous submarine canyons in this area (Figure 1; Graciansky and Lemoine, 1988; Joseph *et al.*, 1989; Friès and Parize, 2003). Nevertheless, the palaeogeography and physiography of the Vocontian Basin could have impacted the heterogeneity of OM sedimentation during GL deposition. The south-eastern part of the basin was farther away from the sedimentary source areas and/or was connected to different sedimentary source area(s). Consequently, the south-eastern part of the basin was better preserved from detrital fluxes (Bréhéret, 1997). Due to the palaeogeography of the Vocontian Basin, it is possible that the watershed that fed the south-eastern part of the basin was more restricted (see Grosheny *et al.*, 2017). This hypothesis is consistent with the distinctive clay assemblages (lack of smectite, see Section 6.1) and IA in the Sauzeries section (see Section 6.5) compared to the eastern sections.

## 8 | CONCLUSIONS

Oceanic Anoxic Events should not be considered as occurring only in oceans or basins with sluggish bottom-water circulations, stratified-water columns and bottom anoxia, if not euxinia. This study demonstrates that OAEs were not uniform but rather heterogeneous. During the OAE 1a, the Vocontian Basin, a marine basin connected to the northern margin of the Tethys Ocean, was (intermittently) stratified, and the deep parts were subjected to redox conditions that were more severe than those affecting the more proximal parts of the basin. The SR was markedly impacted by the occurrences of turbidites, as expected for semi-enclosed basins.

The first take-home message regarding the Vocontian Basin is that water-column stratification did not result from strong surface-water productivity, but rather from: (a) the specific geographical location of the Vocontian Basin, which involved a limited renewal of deep water and an inflow of trace metal and oxygen-depleted waters; and (b) the reputedly high surface-water palaeotemperatures that were prevalent during the OAE 1a. The second take-home message is that turbidite currents and deposits, in addition to diluting OM in the sediments and briefly disrupting the water-column stratification on the upper slope, must have ventilated the sea floor, re-oxidizing the sediment-water interface and the underlying sediments in the relatively long run, even in the deep parts of the basin where reducing conditions prevailed.

No particular evidence has been found that indicates that the Vocontian Basin was markedly impacted by the OAE 1a prevailing in other parts of the Tethys Ocean. This result is rather surprising since the Vocontian Basin was a semi-enclosed basin, connected to an ocean that experienced widespread anoxic conditions. The results presented here suggest that some trace metal and oxygen-depleted waters may have entered the basin during the OAE 1a, but the hypothesis still requires testing. Nevertheless, the deepest part of the basin studied herein must have experienced oxygen-limited conditions, although the geochemical record of such low-oxygenation levels has been locally erased from the sediments by the so-called ‘burn-down effect’. This effect, induced by recurrent turbidites ventilating both the sediment-water interface and the underlying sediments, erased any redox-sensitive element enrichment. Based on the trace element composition of the sediments involved in such turbidite-induced re-oxygenations, one might erroneously conclude that normal, ventilated conditions of deposition prevailed.

### ACKNOWLEDGEMENTS

The authors wish to thank the TOTAL S.A. Company for permitting publishing this article. Marion Delattre, Monique Gentric, Romain Abraham, belonging to the technical staff of the Laboratory of Oceanology and Geosciences (LOG) of the

Earth Sciences Dept. of University of Lille are warmly thanked for their much-appreciated help in the lab, as well as Florence Savignac (ISTeP) for her help in Rock-Eval analyses. We thank our reviewers Alexis Godet and Helmut Weissert, as well as Elias Samankassou (IAS), who helped us improve significantly our manuscript. A special thanks to Vincent Crombez, Tristan Euzen and François Baudin, guest editors of the special issue of International Association of Sedimentologists for their help and advices, as well as to the journal's editorial staff. This work was funded by the TOTAL S.A. Company.

## ORCID

Nicolas Tribovillard  <https://orcid.org/0000-0003-3493-5579>

## REFERENCES

- Ahmed, A.A., Abou-El-Ela, M., Jakupovic, J. and El-Din, A.A. (1990) Eudesmanolides and other constituents from *Artemisia herba-alba*. *Phytochemistry*, 29, 3661–3663.
- Alexander, G., Hazai, I., Grimalt, J. and Albaigés, J. (1987) Occurrence and transformation of phyllocladanes in brown coals from Nograd Basin, Hungary. *Geochimica et Cosmochimica Acta*, 51(8), 2065–2073.
- Algeo, T.J. and Lyons, T.W. (2006) Mo-total organic carbon covariation in modern anoxic marine environments: implications for analysis of paleoredox and paleohydrographic. *Paleoceanography*, 21(1), PA1016.
- Algeo, T.J. and Tribovillard, N. (2009) Environmental analysis of paleoceanographic systems based on molybdenum–uranium covariation. *Chemical Geology*, 268, 211–225.
- Ando, T., Sawada, K., Okano, K., Takashima, R. and Nishi, H. (2017) Marine primary producer community during the mid-Cretaceous oceanic events (OAEs) 1a, 1b and 1d in the Vocontian Basin (SE France) evaluated from triaromatic steroids in sediments. *Organic Geochemistry*, 106, 13–24.
- Arnaud-Vanneau, A. and Arnaud, H. (1991) Sédimentation et variations relatives du niveau de la mer sur les plates-formes carbonatées du Berriasien-Valanginien et du Barrémien dans les massifs subalpins septentrionaux et le Jura (SE de la France). *Bulletin de la Société Géologique de France*, 162, 535–545.
- Arthur, M.A., Dean, W.E. and Pratt, L.M. (1988) Geochemical and climatic effects of increased marine organic carbon burial at the Cenomanian/Turonian boundary. *Nature*, 335, 714–717.
- Arthur, M.A., Dean, W.E. and Schlanger, S.O. (1985) Variations in the global carbon cycle during the Cretaceous related to climate, volcanism, and changes in atmospheric CO<sub>2</sub>: Natural variations Archean to present. In: Sundquist, E.T. and Broecker, W.S. (Eds.) *The Carbon Cycle and Atmospheric CO<sub>2</sub>. Monographs of the American Geophysical Union*, 32, 504–529.
- Arthur, M.A., Jenkyns, H.C., Brumsack, H.J. and Schlanger, S.O. (1990) Stratigraphy, geochemistry, and paleoceanography of organic carbon-rich Cretaceous sequences. In: Ginsburg, R.N. and Beaudoin, B. (Eds.) *Cretaceous Resources, Events and Rhythms: Background and Plans for Research. NATO ASI Series C 304*, 75–119.
- Arthur, M.A. and Schlanger, S.O. (1979) Cretaceous “Oceanic Anoxic Events” as causal factors in development of reef-reservoired giant oil fields. *American Association of Petroleum Geologists, Bulletin*, 63, 870–885.
- Attewell, P.B. and Farmer, I.W. (1976) *Principles of Engineering Geology*. London: Chapman and Hall.
- Baudin, F., Tribovillard, N. and Trichet, J. (2017) *Géologie de la matière organique*, 2nd edition. Paris: Vuibert and Société Géologique de France, 263 p.
- Baudrimont, A.F. and Dubois, P. (1977) Un bassin mésogéen du domaine péri-alpin: le Sud-Est de la France. *Bulletin des Centres de Recherches Exploration Production Elf-Aquitaine*, 1, 261–308.
- Beaudoin, B. and Friès, G. (1984) Phénomènes de resédimentation. Crétacé inférieur subalpin. 5<sup>ième</sup> Congrès Européen de Sédimentologie, Marseille, Livret-guide, Excursion, no. 6, 51 pp.
- Beaudoin, B., Friès, G., Joseph, P., Bouchet, R. and Cabrol, C. (1986) Tectonique synsédimentaire crétacée à l’Ouest de la Durance (S.E. France). *Comptes Rendus de l’Académie des Sciences de Paris*, 303, 713–718.
- Behar, F., Beaumont, V., Pentead, H.L. and De, B. (2001) Technologie Rock-Eval 6: Performances et Développements. *Oil and Gas Science and Technology*, 56(2), 111–134.
- Bénard, F., de Charpal, O., Mascle, A. and Trémolières, P. (1985) Mise en évidence d’une phase de serrage Est-Ouest au Crétacé inférieur en Europe de l’Ouest. *Comptes Rendus de l’Académie des Sciences de Paris*, 300, 765–768.
- Blumenberg, M., Mollenhauer, G., Zabel, M., Reimer, A. and Thiel, V. (2010) Decoupling of bio- and geohopanoids in sediments of the Benguela Upwelling System (BUS). *Organic Geochemistry*, 41, 1119–1129.
- Bodin, S., Godet, A., Westermann, S. and Föllmi, K.B. (2013) Secular change in northwestern Tethyan water-mass oxygenation during the late Hauterivian-early Aptian. *Earth and Planetary Science Letters*, 374, 121–131.
- Bohacs, K.M., Grabowski, G.J., Carroll, A.R., Mankiewicz, P.J., Miskell-Gerhardt, K.J., Schwalbach, J.R., Wegner, M.B. and Simo, J.A.T. (2005) Production, Destruction, and Dilution—The Many Paths to Source-Rock Development. In: Harris, N.B. (Eds) *The Deposition of Organic-carbon-rich Sediments: Models, Mechanisms and Consequences*. Tulsa, OK: Special Publications of SEPM, pp. 31–101.
- Bonin, A., Pucéat, E., Vennin, E., Mattioli, E., Aurell, M., Joachimski, M. et al. (2016) Cool episode and platform demise in the Early Aptian: new insights on the links between climate and carbonate production. *Paleoceanography*, 31, 66–80.
- Bottini, C., Erba, E., Tiraboschi, D., Jenkyns, H.C., Schouten, S. and Sinninghe Damsté, J.S. (2015) Climate variability and ocean fertility during the Aptian Stage. *Climate of the Past*, 11(3), 383–402.
- Bouma, A.H. (1962) Sedimentology of some flysch deposits. A graphic approach of facies interpretation. PhD thesis, University of Utrecht, Amsterdam, Elsevier Publishers, 168 pp.
- Bout-Roumazielles, V., Eisa, C., Laurent, L. and Pierre, D. (1999) Clay mineral evidence of nepheloid layer contributions to the heinrich layers in the Northwest Atlantic. *Palaeogeography, Palaeoclimatology, Palaeoecology*, 146(1–4), 211–228.
- Bralower, T.J., Arthur, M.A., Leckie, R.M., Sliter, W.V., Allard, D.J. and Schlanger, S.O. (1994) Timing and paleoceanography of oceanic dysoxia/anoxia in the late Barremian to early Aptian (Early Cretaceous). *Palaios*, 9, 335–369.
- Bralower, T.J., Cobabe, E., Clement, B., Sliter, W.V., Osburn, C.L. and Longoria, J. (1999) The record of global change in mid-Cretaceous

- (Barremian-Albian) sections from Sierra Madre, northeastern Mexico. *Journal of Foraminiferal Research*, 29, 418–437.
- Bralower, T.J., Sliter, W.V., Arthur, M.A., Leckie, R.M., Allard, D.J. and Schlanger, S.O. (1993) Dysoxic/anoxic episodes in the Aptian-Albian (Early Cretaceous). In: Pringle, M.S., Sager, W.W., Sliter, W.V. and Stein, S. (Eds.) *The Mesozoic Pacific: Geology, Tectonics, and Volcanism. Geophysical Monograph Series*, 77, 5–37. Washington, DC: AGU.
- Bréhéret, J.G. (1994) The Mid-Cretaceous organic-rich sediments from the Vocontian Zone of the French Southeast Basin. In: Mascle, A. (Ed.) *Hydrocarbon and Petroleum Geology of France, Special Publication EAPG 4*, 295–320.
- Bréhéret, J.G. (1997) L'Aptien et l'Albien de la fosse vocontienne (des bordures au bassin). Evolution de la sédimentation et enseignements sur les évènements anoxiques. PhD thesis, University of Tours, France. Publication Société Géologique du Nord 25, 614 pp.
- Brocks, J.J. and Schaeffer, P. (2008) Okenane, a biomarker for purple sulfur bacteria (Chromatiaceae), and other new carotenoid derivatives from the 1640 Ma Barney Creek Formation. *Geochimica et Cosmochimica Acta*, 72, 1396–1414.
- Chamley, H. (1989) *Clay Sedimentology*. Berlin: Springer Verlag.
- Charbonnier, G. and Föllmi, K.B. (2017) Mercury enrichments in lower Aptian sediments support the link between Ontong Java large igneous province activity and oceanic anoxic episode 1a. *Geology*, 45, 63–66.
- Clifford, D.J., Clayton, J.L. and Sinninghe Damsté, J.S. (1998) 2,3,6-/3,4,5-trimethyl substituted diaryl carotenoid derivatives (Chlorobiaceae) in petroleum of the Belarussian Pripyat River Basin. *Organic Geochemistry* 29, 1253–1267.
- Coccioni, R., Nesci, O., Tramontana, M., Wezel, F.-C. and Moretti, E. (1987) Descrizione di un livello-guida “radiolaritico-bituminoso-ittiolitico” alla base delle Marne a Fucoidi nell'Appennino umbro-marchigiano. *Bollettino della Società Geologica Italiana*, 106, 183–192.
- Cotillon, P. (2010) Sea bottom current activity recorded on the southern margin of the Vocontian basin (southeastern France) during the lower Aptian. Evidence for a climatic signal. *Bulletin de la Société Géologique de France*, 181(1), 3–18.
- Cowie, G.L., Hedges, J.I., Prah, F.G. and De Lange, G.J. (1995) Elemental and major biochemical changes across an oxidation front in a relict turbidite: an oxygen effect. *Geochimica et Cosmochimica Acta*, 59(1), 33–46.
- Cranwell, P.A., Eglinton, G. and Robinson, N. (1987) Lipids of aquatic organisms as potential contributors to lacustrine sediments-II. *Organic Geochemistry*, 11, 513–527.
- Creaney, S. and Passey, Q.R. (1993) Recurring patterns of total organic carbon and source rock quality within a sequence stratigraphic framework. *American Association of Petroleum Geologists Bulletin*, 77, 386–401.
- Dauphin, L. (2002) Litho-, bio- et chronostratigraphie comparées dans le bassin vocontien, à l'Aptien. PhD thesis, University of Lille I, France, 516 pp.
- Deconinck, J.-F. (1984) Sédimentation et diagénèse des minéraux argileux du Jurassique supérieur-Crétacé dans le Jura meridional et le domaine subalpine (France Sud-Est); comparaison avec le domaine Atlantique Nord. PhD thesis, University of Lille, 150 pp.
- Deconinck, J.F. (1987) Identification de l'origine détritico ou diagénétique des assemblages argileux: le cas des alternances marne-calcaire du Crétacé inférieur subalpin. *Bulletin de la Société Géologique de France*, 3, 139–145.
- Delamette, M. (1990) Aptian, Albian and Cenomanian microbialites from the condensed phosphatic deposits of the Helvetic shelf, Western Alps. *Eclogae Geologicae Helvetiae*, 83(1), 99–121.
- Dunoyer de Seconzac, G. (1969). Les minéraux argileux dans la diagénèse. Passage au métamorphisme. Mémoires du service de la carte géologique d'Alsace et de la Lorraine, vol. 29, Strasbourg, 320pp.
- Eglinton, G. and Hamilton, R.J. (1967) Leaf epicuticular waxes. *Science*, 156, 1322–1335.
- Emeiss, K.-C. and Weissert, H. (2009) Tethyan-Mediterranean organic carbon-rich sediments from Mesozoic black shales to sapropels. *Sedimentology*, 56(1), 247–266.
- Erba, E. (1994) Nannofossils and superplumes: the early Aptian “nannocoid crisis”. *Paleoceanography*, 9(3), 483–501.
- Erba, E., Bottini, C., Weissert, H.J. and Keller, C.E. (2010) Calcareous nannoplankton response to surface-water acidification around oceanic anoxic event 1a. *Science*, 329, 428–432.
- Erba, E., Channell, J.E.T., Claps, M., Jones, C., Larson, R., Opdyke, B. et al. (1999) Integrated stratigraphy of the Cisono Apticore (southern Alps, Italy): a “reference section” for the Barremian-Aptian interval at low latitudes. *Journal of Foraminiferal Research*, 29, 371–391.
- Erba, E., Duncan, R.A., Bottini, C., Tiraboschi, D., Weissert, H., Jenkyns, H.C. et al. (2015) Environmental consequences of Ontong Java Plateau and Kerguelen plateau volcanism. *Geological Society of America Special Paper*, 511, 271–303.
- Espitalié, J., Deroo, G. and Marquis, F. (1985) La pyrolyse Rock-Eval et ses applications. *Revue de l'Institut Français du Pétrole*, 40, 563–579.
- Espitalié, J. (1993) Rock Eval pyrolysis. In: Bordenave, M.L. (Ed.) *Applied Petroleum Geochemistry*. Paris: Technip, pp. 237–261.
- Esquivin, J. (1969) Influence de la composition chimique des illites sur leur cristallinité. *Bulletin du Centre de Recherches de Pau-SNPA*, 3, 147–153.
- Ferry, S. (2017) Summary on Mesozoic carbonate deposits of the Vocontian Trough (Sub-alpine Chains). In: Granier, B. (Ed.) *Some Key Lower Cretaceous Sites in Drôme (SE France)*. Madrid: Carnets de Géologie. CG2017\_B01, pp. 9–42.
- Föllmi, K.B. (2008) A synchronous, middle early Aptian age for the demise of the Helvetic Urganian platform related to the unfolding oceanic anoxic event 1a ('Selli event'). *Revue de Paléobiologie*, 27, 461–468.
- Föllmi, K.B. (2012) Early Cretaceous life, climate and anoxia. *Cretaceous Research*, 35, 230–257.
- Föllmi, K.B. (1995) 160 m.y. record of marine sedimentary phosphorous burial: coupling of climate and continental weathering under greenhouse and icehouse conditions. *Geology*, 23, 859–862.
- Föllmi, K.B., Bôle, M., Jammet, N., Froidevaux, P., Godet, A., Bodin, S. et al. (2012) Bridging the Faraoni and Selli oceanic anoxic events: Late Hauterivian to early Aptian dysaerobic to anaerobic phases in the Tethys. *Climate of the Past*, 8, 171–189.
- Föllmi, K.B., Delamette, M. and Ouwehand, P.J. (2011) Aptian to Cenomanian deeper-water hiatal stromatolites from the Northern Tethyan Margin. In: Tewari, V. and Seckbach, J. (Eds.) *Stromatolites: Interaction of Microbes with Sediments. Cellular Origin, Life in Extreme Habitats and Astrobiology*, vol. 18. Dordrecht: Springer, pp. 159–186.
- Föllmi, K.B., Godet, A., Bodin, S. and Linder, P. (2006) Interactions between environmental change and shallow-water carbonate build-up along the northern Tethyan margin and their impact on the Early Cretaceous carbon-isotope record. *Paleoceanography*, 21, PA4211.

- Föllmi, K.B., Weissert, H., Bispin, M. and Funk, H. (1994) Phosphogenesis, carbon-isotope stratigraphy, and carbonate-platform evolution along the Lower Cretaceous northern Tethyan margin. *Geological Society of America, Bulletin*, 106, 729–746.
- Frau, C., Pictet, A., Spangenberg, J.E., Masse, J.-P., Tendil, A.J.-B. and Lanteaume, C. (2017) New insights on the age of the post-Urgonian marly cover of the Apt region (Vaucluse, SE France) and its implication on the demise of the North Provence carbonate platform. *Sedimentary Geology*, 359, 44–61.
- Friès, G. and Parize, O. (2003) Anatomy of ancient passive margin slope systems: Aptian gravity-driven deposition on the Vocontian palaeo-margin, western Alps, south-east France. *Sedimentology*, 50(6), 1231–1270.
- Friès, G. (1987) Dynamique du bassin subalpin méridional de l'Aptien au Cénomani. PhD thesis, University of Paris 6, France. Mémoire des. Sciences de la Terre ENS Mines Paris 4,370 pp.
- Ghirardi, J., Deconinck, J.-F., Pellenard, P., Martinez, M., Bruneau, L., Amiotte-Suchet, P. *et al.* (2014) Multi-proxy orbital chronology in the aftermath of the Aptian Oceanic anoxic event 1a: Palaeoceanographic implications (Serre Chaitieu section, Vocontian Basin, SE France). *Newsletters on Stratigraphy*, 47(3), 247–262.
- Gibbs, S.J., Robinson, S.A., Bown, P.R., Dunkley Jones, T. and Henderiks, J. (2011) Comment on "Calcareous Nannoplankton response to surface-water acidification around oceanic anoxic event 1a". *Science*, 332, 175b.
- Gignoux, M. (1925) *Géologie Stratigraphique*. Paris: Masson et Cie.
- Giraud, F., Pittet, B., Grosheny, D., Baudin, F., Lécuyer, C. and Sakamoto, T. (2018) The palaeoceanographic crisis of the early Aptian (OAE 1a) in the Vocontian Basin (SE France). *Palaeogeography, Palaeoclimatology, Palaeoecology*, 511, 483–505.
- Goldberg, K. and Humayun, M. (2010) The applicability of the chemical index of alteration as a paleoclimatic indicator: an example from the Permian of the Paraná Basin, Brazil. *Palaeogeography, Palaeoclimatology, Palaeoecology*, 293, 175–183.
- de Graciansky, P.C. and Lemoine, M. (1988) Early Cretaceous extensional tectonics in the southwestern French Alps: a consequence of North-Atlantic rifting during Tethyan spreading. *Bulletin de la Société Géologique de France*, 4(5), 733–737.
- Grosheny, D., Ferry, S., Lécuyer, C., Thomas, A. and Desmares, D. (2017) The Cenomanian-Turonian Boundary Event (CTBE) on the southern slope of the Subalpine Basin (SE France) and its bearing on a probable tectonic pulse on a larger scale. *Cretaceous Research*, 72, 39–65.
- Haq, B.U. (2014) Cretaceous eustasy revisited. *Global and Planetary Change*, 113, 44–58.
- Haq, B.U., Hardenbol, J. and Vail, P.R. (1987) Chronology of fluctuating sea levels since the Triassic. *Science*, 235, 1156–1167.
- Harvey, H.R. and McManus, G.B. (1991) Marine ciliates as a widespread source of tetrahymanol and hopan-3 $\beta$ -ol in sediments. *Geochimica et Cosmochimica Acta*, 55, 3387–3390.
- Hatcher, P.G. and Clifford, D.J. (1997) The organic geochemistry of coal: from plant materials to coal. *Organic Geochemistry*, 27, 251–274.
- Heimhofer, U., Hochuli, P.A., Herrle, J.O., Andersen, N. and Weissert, H. (2004) Absence of major vegetation and palaeoatmospheric pCO<sub>2</sub> changes associated with oceanic anoxic event 1a (Early Aptian, SE France). *Earth Planetary Science Letters*, 223, 303–318.
- Heimhofer, U., Hochuli, P.A., Herrle, J.O. and Weissert, H. (2006) Contrasting origins of Early Cretaceous black shales in the Vocontian basin: Evidence from palynological and calcareous nannofossil records. *Palaeogeography, Palaeoclimatology, Palaeoecology*, 235, 93–109.
- Herrle, J.O. and Mutterlose, J. (2003) Calcareous nannofossils from the Aptian – early Albian of SE France: Paleocological and biostratigraphic implications. *Cretaceous Research*, 24, 1–22.
- Hibsch, C., Kandel, D., Montenat, C. and Ott d'Estevou, P. (1992) Événements tectoniques crétacés dans la partie méridionale du bassin subalpin (massif Ventoux-Lure et partie orientale de l'arc de Castellane, SE France). Implications géodynamiques. *Bulletin de la Société Géologique de France*, 163, 147–158.
- Hoefs, M.J.L., Rijpstra, W.I.C. and Sinninghe Damsté, J.S. (2002) The influence of oxic degradation on the sedimentary biomarker record I: evidence from Madeira Abyssal plain turbidites. *Geochimica et Cosmochimica Acta*, 66(15), 2719–2735.
- Huang, C., Hinnov, L., Fischer, A.G., Grippo, A. and Herbert, T. (2010) Astronomical tuning of the Aptian Stage from Italian reference sections. *Geology*, 38(10), 899–902.
- Huck, S., Heimhofer, U., Rameil, N., Bodin, S. and Immenhauser, A. (2011) Strontium and carbon-isotope chronostratigraphy of Barremian-Aptian shoal-water carbonates: Northern Tethyan platform drowning predates OAE 1a. *Earth and Planetary Science Letters*, 304(3), 547–558.
- Immenhauser, A., Hillgärtner, H. and van Bentum, E. (2005) Microbial-foraminiferal episodes in the Early Aptian of the southern Tethyan margin: ecological significance and possible relation to oceanic anoxic event 1a. *Sedimentology*, 52, 77–99.
- Jacquín, T. and de Graciansky, P.C. (1988) Cyclic fluctuations of anoxia during Cretaceous time in the South Atlantic Ocean. *Marine and Petroleum Geology*, 5(4), 359–369.
- Jenkyns, H.C. (1999) Mesozoic anoxic events and palaeoclimate. *Zentralblatt für Geologie und Paläontologie*, 7–9, 943–949.
- Jenkyns, H.C. (2003) Evidence for rapid climate change in the Mesozoic-Palaeogene greenhouse world. *Royal Society of London Transactions Series A*, 361(1), 1885–1916.
- Jenkyns, H.C. (2010) Geochemistry of oceanic anoxic events. *Geochemistry, Geophysics, Geosystems*, 11(3), 1–30.
- Jiang, C., Chen, Z., Lavoie, D., Percival, J.B. and Kabanov, P. (2017) Mineral carbon MinC(%) from rock-eval analysis as a reliable and cost-effective measurement of carbonate contents in shale source and reservoir rocks. *Marine and Petroleum Geology*, 83, 184–194.
- Joseph, P., Beaudoin, B., Friès, G. and Parize, O. (1989) Les vallées sous-marines enregistrent au Crétacé inférieur le fonctionnement en blocs basculés du domaine vocontien. *Comptes Rendus de l'Académie des Sciences de Paris*, 309, 1031–1038.
- Junior, G.R.S., Santos, A.L.S., de Lima, S.G., Lopes, J.A.D., Reis, F.A.M., Neto, E.V.S. *et al.* (2013) Evidence for euphotic zone anoxia during the deposition of Aptian source rocks based on aryl isoprenoids in petroleum, Sergipe Alagoas Basin, northeastern Brazil. *Organic Geochemistry*, 63C, 94–104.
- Khaled, H., Chaabani, F., Boulvain, F. and Mansoura, M. (2017) Characterization of the Late Barremian in north central Tunisia: is it a prelude to the oceanic anoxic event 1a? *Journal of African Earth Sciences*, 125, 177–190.
- Köbler, P., Herrle, J.O., Appel, E., Erbacher, J. and Hemleben, C. (2001) Magnetic records of climatic cycles from mid-Cretaceous hemipelagic sediments of the Vocontian Basin, SE France. *Cretaceous Research*, 22, 321–331.
- Koopmans, M.P., Köster, J., van Kaam-Peters, H.M.E., Kenig, F., Schouten, S., Hartgers, W.A. *et al.* (1996) Diagenetic and catagenetic

- products of Isorenieratene: molecular indicators for photic zone anoxia. *Geochemica et Cosmochimica Acta*, 60, 4467–4496.
- Kübler, B. (1967) Anchimétamorphisme et schistosité. *Bulletin du Centre de Recherches de Pau-SNPA*, 1, 259–278.
- Kübler, B. and Jaboyedoff, M. (2000) Illite crystallinity. *Comptes Rendus de l'Académie des Sciences – Series IIA – Earth and Planetary Science*, 331(2), 75–89.
- Leckie, R.M., Bralower, T.J. and Cashman, R. (2002) Oceanic anoxic events and plankton evolution: biotic response to tectonic forcing during the mid-Cretaceous. *Paleoceanography*, 17(3), PA000623.
- Levert, F. and Ferry, S. (1987) L'apport argileux dans le bassin mésozoïque subalpin. Quantification et problème d'altération de l'héritage. *Géol Alp Mém Hors-Série*, 13, 209–2013.
- Levert, J. and Ferry, S. (1988) Diagenèse argileuse complexe dans le Mésozoïque subalpin révélée par cartographie des proportions relatives d'argiles selon des niveaux isochrones. *Bulletin de la Société Géologique de France*, 4, 1029–1038.
- Liu, N., Zhang, L., Wang, S., Wang, X.-N., Wang, S.-Q. and Lou, H.-X. (2012) Eudesmane-type sesquiterpenes from the liverwort *Apomarsipella revolute*. *Phytochemistry Letters*, 5, 346–350.
- Malinverno, A., Erba, E. and Herbert, T.D. (2010) Orbital tuning as an inverse problem: chronology of the early Aptian oceanic anoxic event 1a (Selli level) in the Cismon APTICORE. *Paleoceanography*, 25, PA2203.
- Malkoc, M., Mutterlose, J. and Pauly, S. (2010) Timing of the early Aptian  $\delta^{13}\text{C}$  excursion in the Boreal Realm. *Newsletter on Stratigraphy*, 43, 251–273.
- Masse, J.-P., Bouaziz, S., Amon, E.O., Baraboshin, E., Tarkowski, R.A., Bergerat, F. et al. (2000) Early Aptian (112–114 Ma), map 13. In: Dercourt, J., Gaetani, M., Vrielynck, B., Barrier, E., Bijou-Duval, B., Brunet, M.F., Cadet, J.P., Crasquin, S. and Sandulescu, M. (Eds.) *Atlas Peri-Tethys: Palaeoenvironmental Maps, Explanatory Notes*. Paris: Commission de la carte géologique du monde, 268 pp.
- Masse, J.-P. and Fenerci-Masse, M. (2011) Drowning discontinuities and stratigraphic correlation in platform carbonates. The late Barremian- early Aptian record of southeast France. *Cretaceous Research*, 32, 659–684.
- Masse, J.-P. and Philip, J. (1976) Paléogéographie et tectonique du Crétacé moyen en Provence: révision du concept d'isthme durancien. *Revue de géologie dynamique et de géographie physique*, 18, 49–66.
- McCave, I.N., Manighetti, B. and Robinson, S.G. (1995) Sortable silt and fine sediment size/composition slicing: parameters for palaeo-current speed and palaeoceanography. *Paleoceanography*, 10(3), 593–610.
- McLennan, S.M. (2001) Relationships between the trace element composition of sedimentary rocks and upper continental crust. *Geochemistry Geophysics Geosystems*, 2, 1021.
- Méhay, S., Keller, C.E., Bernasconi, S.M., Weissert, H., Erba, E., Bottini, C. et al. (2009) A volcanic  $\text{CO}_2$  pulse triggered the Cretaceous oceanic anoxic event 1a and a biocalcification crisis. *Geology*, 37, 819–822.
- Menegatti, A.P., Weissert, H., Brown, R.S., Tyson, R.V., Farrimond, P., Strasser, A. et al. (1998) High-resolution  $\delta^{13}\text{C}$  stratigraphy through the early Aptian “Livello Selli” of the Alpine Tethys. *Paleoceanography*, 13(5), 530–545.
- Meyers, P.A., Silliman, J.E. and Shaw, T.J. (1996) Effects of turbidity flows on organic matter accumulation, sulfate reduction, and methane generation in deep-sea sediments on the Iberia Abyssal Plain. *Organic Geochemistry*, 25(1–2), 69–78.
- Middelburg, J.J. and De Lange, G.J. (1988) Geochemical characteristics as indicators of the provenance of Madeira abyssal plain turbidites. A statistical approach. *Oceanologica Acta*, 11(2), 159–165.
- Montero-Serrano, J.C., Föllmi, K.B., Adatte, T., Spangenberg, J.E., Tribouillard, N., Fantasia, A. et al. (2015) Continental weathering and redox conditions during the early Toarcian Oceanic Anoxic Event in the northwestern Tethys: insight from the Posidonia Shale section in the Swiss Jura Mountains. *Palaeogeography, Palaeoclimatology, Palaeoecology*, 429, 83–99.
- Moreno-Bedmar, J.A., Company, M., Bover-Arnal, T., Salas, R., Delanoy, G., Martínez, R. et al. (2009) Biostratigraphic characterization by means of ammonoids of the lower Aptian Oceanic Anoxic Event (OAE 1a) in the eastern Iberian Chain (Maestrat Basin, eastern Spain). *Cretaceous Research*, 30, 864–872.
- Moullade, M., Kuhnt, W., Bergen, J.A., Masse, J.P. and Tronchetti, G. (1998a) Correlation of biostratigraphic and stable isotope events in the Aptian historical stratotype of La Bédoule (south-east France). *Comptes Rendus de l'Académie des Sciences de Paris*, 327, 693–698.
- Moullade, M., Masse, J.P., Tronchetti, G., Kuhnt, W., Ropolo, P., Bergen, J.A. et al. (1998b) Le stratotype historique de l'Aptien inférieur (région de Cassis-La Bédoule, SE France): synthèse stratigraphique. *Géologie Méditerranéenne*, 25(3–4), 289–298.
- Nesbitt, H.W. and Young, G.M. (1982) Early Proterozoic climates and plate motions inferred from major element chemistry of lutites. *Nature*, 299, 715–717.
- Noble, R.A. (1986) A geochemical study of bicyclic alkanes and diterpenoid hydrocarbon in crude oils, sediment and coals. PhD thesis, University of Western Australia, Australia.
- Okano, K., Sawada, K., Takashima, R., Nishi, H. and Okada, H. (2008) Further examples of archaeal-derived hydrocarbons in mid-Cretaceous oceanic anoxic event (OAE) 1b sediments. *Organic Geochemistry*, 39, 1088–1091.
- Ouirisson, G., Albrecht, P. and Rohmer, M. (1979) The Hopanoids: palaeochemistry and biochemistry of a group of natural products. *Pure and Applied Chemistry*, 51, 709–729.
- Pancost, R.D., Crawford, N., Magness, S., Turner, A., Jenkyns, H.C. and Maxwell, J.R. (2004) Further evidence for the development of photic-zone euxinic conditions during Mesozoic oceanic anoxic events. *Journal of the Geological Society, London*, 161, 353–364.
- Pastorova, I., Botto, R.E., Arisz, P.W. and Boon, J.J. (1994) Cellulose char structure: a combined analytical Py-GC-MS, FTIR, and NMR study. *Carbohydrate Research*, 262(1), 27–47.
- Peters, K., Walters, C. and Moldowan, J. (2005) *The Biomarker Guide: Biomarkers and Isotopes in the Environment and Human History*, 2nd edition. New York: Cambridge University Press.
- Pictet, A., Delanoy, G., Adatte, T., Spangenberg, J.E., Baudouin, C., Boselli, P. et al. (2015) Three successive phase of platform demise during the early Aptian and their association with the oceanic Selli episode (Ardèche, France). *Palaeogeography, Palaeoclimatology, Palaeoecology*, 418, 101–125.
- Prahl, F.G., Cowie, G.L., De Lange, G.J. and Sparrow, M.A. (2003) Selective organic matter preservation in “burn-down” turbidites on the Madeira Abyssal Plain. *Paleoceanography*, 18(2), 1052.
- Prahl, F.G., De Lange, G.J., Scholten, S. and Cowie, G.L. (1997) A case of post-depositional aerobic degradation of terrestrial organic matter in turbidite deposits from the Madeira Abyssal Plain. *Organic Geochemistry*, 27(3–4), 141–152.

- Radke, M., Vriend, S.P. and Ramanampisoa, L.R. (2000) Alkyldibenzofurans in terrestrial rocks: influence of organic facies and maturation. *Geochimica et Cosmochimica Acta*, 64, 275–286.
- Radke, M., Welte, D.H. and Willsch, H. (1986) Maturity parameters based on aromatic hydrocarbons: influence of the organic matter type. *Organic Geochemistry*, 10, 51–63.
- Quijada, M., Riboulleau, A., Guerardel, Y., Monnet, Y. and Tribouillard, N. (2015) Neutral aldoses derived from sequential acid hydrolysis of sediments as indicators of diagenesis over 120,000 years. *Organic Geochemistry*, 81, 53–63.
- Reboulet, S., Szives, O., Aguirre-Urreta, B., Barragán, R., Company, M., Idakieva, V. et al. (2014) Report on the 5th International Meeting of the IUGS Lower Cretaceous Ammonite Working Group, the Kilian Group (Ankara, Turkey, 31st August 2013). *Cretaceous Research*, 50, 126–137.
- Riboulleau, A., Bout-Roumazeilles, V. and Tribouillard, N. (2014) Controls on detrital sedimentation in the Cariaco Basin during the last climatic cycle: insight from clay minerals. *Quaternary Science Reviews*, 94, 62–73.
- Ricou, L.E. and de Lamotte, F. (1986) Décrochement senestre médio-crétaïc entre Provence et Alpes-Maritimes (Alpes occidentales, France). *Revue de Géologie Dynamique et de Géographie Physique, Paris*, 27(3–4), 237–245.
- Rohrsen, M., Love, G.D., Fischer, W., Finnegan, S. and Fike, D.A. (2013) Lipid biomarkers record fundamental changes in the microbial community structure of tropical seas during the Late Ordovician Hirnantian glaciation. *Geology*, 41, 127–130.
- Romero-Sarmiento, M.-F., Riboulleau, A., Vecoli, M., Laggoun-Défarge, F. and Versteegh, G.J.M. (2011) Aliphatic and aromatic biomarkers from Carboniferous coal deposits at Dunbar (East Lothian, Scotland): palaeobotanical and palaeoenvironmental significance. *Palaeogeography, Palaeoclimatology, Palaeoecology*, 309, 309–326.
- Rubino, J.-L. (1989) Introductory remarks on Upper Aptian to Albian siliciclastic/carbonate depositional sequences. In: Ferry, S. and Rubino, J.-L. (Eds) *Mesozoic Eustasy on Western Tethyan Margins*. Post-Meeting Field Trip in the “Vocontian Trough”. ASF, Publ. Spéc. 12, 28–45.
- Sáenz, J.P., Wakeham, S.G., Eglinton, T.I. and Summons, R.E. (2011) New constraints on the provenance of hopanoids in the marine geologic record: bacteriohopanepolyols in marine suboxic and anoxic environments. *Organic Geochemistry*, 42, 1351–1362.
- Sageman, B.B., Murphy, A.E., Werne, J.P., Ver Straeten, C.A., Hollander, D.J. and Lyons, T.W. (2003) A tale of shales: the relative roles of production, decomposition, and dilution in the accumulation of organic-rich strata, Middle-Upper Devonian, Appalachian basin. *Chemical Geology*, 195, 229–273.
- Sanfourche, J. and Baudin, F. (2001) La genèse des événements anoxiques de la période moyenne du Crétacé. Examen de l’hypothèse du mécroclimatisme océanique. *Annales de la Société Géologique du Nord*, T.8 (2e, série), 107–119.
- Schaeffer, P., Adam, P., Wehrung, P. and Albrecht, P. (1997) Novel aromatic carotenoid derivatives from sulfur photosynthetic bacteria in sediments. *Tetrahedron Letters*, 38, 8413–8416.
- Schlanger, S.O. and Jenkyns, H.C. (1976) Cretaceous oceanic anoxic event: causes and consequences. *Geologie en Mijnbouw*, 55, 179–188.
- Schwark, L. and Frimmel, A. (2004) Chemostratigraphy of the Posidonia Black Shale, SW-Germany. *Chemical Geology*, 206, 231–248.
- Seifert, W.K. and Michael Moldowan, J. (1978) Applications of steranes, terpanes and monoaromatics to the maturation, migration and source of crude oils. *Geochimica et Cosmochimica Acta*, 42, 77–95.
- Sinninghe Damsté, J.S., Kenig, F., Koopmans, M.P., Köster, J., Schouten, S., Hayes, J.M. et al. (1995) Evidence for gammacerane as an indicator of water column stratification. *Geochimica et Cosmochimica Acta*, 59(9), 1895–1900.
- Sinninghe Damsté, J.S. and Koopmans, M.P. (1997) The fate of carotenoids in sediments: an overview. *Pure and Applied Chemistry*, 69, 2067–2074.
- Souquet, P. (1978) Présentation d’une nouvelle esquisse structurale de la chaîne alpine des Pyrénées. *Bulletin de la Société Géologique de France*, 7(5), 711–712.
- Sperazza, M., Moore, J.N. and Hendrix, M.S. (2004) High-resolution particle size analysis of naturally occurring very fine-grained sediment through laser diffractometry. *Journal of Sedimentary Research*, 74(5), 736–743.
- Stampfli, G.M., Mosar, J., Marquer, D., Marchand, R., Baudin, T. and Borel, G. (1998) Subduction and obduction processes in the Swiss Alps. *Tectonophysics*, 296, 159–204.
- Stefanova, M., Simoneit, B., Stojanova, G. and Nosyrev, I.E. (1995) Composition of the extract from a Carboniferous bituminous coal: 1. Bulk and molecular constitution. *Fuel*, 74(8), 1194–1199.
- Stein, M., Föllmi, K.B., Westermann, S., Godet, A., Adatte, T., Matera, V. et al. (2011) Progressive palaeoenvironmental change during the Late Barremian-Early Aptian as prelude to Oceanic Anoxic Event 1a: evidence from the Gorgo a Cerbara section (Umbria-Marche basin, central Italy). *Palaeogeography, Palaeoclimatology, Palaeoecology*, 302(3–4), 396–406.
- Stein, M., Westermann, S., Adatte, T., Matera, V., Fleitmann, D., Spangenberg, J.E. et al. (2012) Late Barremian-Early Aptian paleoenvironmental change: the Cassis-La Bédoule section (SE France). *Cretaceous Research*, 37, 209–222.
- Stein, R., Rullkötter, J. and Welte, D.H. (1986) Accumulation of organic-carbon-rich sediments in the Late Jurassic and Cretaceous Atlantic ocean – a synthesis. *Chemical Geology*, 56, 1–32.
- Summerhayes, C.P. (1981) Organic facies of middle cretaceous black shales in deep North Atlantic. *American Association of Petroleum Geologists Bulletin*, 65(11), 2364–2380.
- Taylor, S.R. and McLennan, S.M. (1985) *The Continental Crust: Its Composition and Evolution*. Oxford: Blackwell, 312 pp.
- Tejada, M.L.G., Katsuhiko, S., Kuroda, J., Coccioni, R., Mahoney, J.J., Ohkouchi, N. et al. (2009) Ontong Java Plateau eruption as a trigger for the early Aptian oceanic anoxic event. *Geology*, 37, 855–858.
- Ten Haven, H.L., Rohmer, M., Rullkötter, J. and Bissleret, P. (1989) Tetrahymanol, the most likely precursor of gammacerane, occurs ubiquitously in marine sediments. *Geochimica et Cosmochimica Acta*, 53, 3073–3079.
- Thomson, J., Jarvis, I., Green, D.R.H., Green, D.A. and Clayton, T. (1998) Mobility and immobility of redox-sensitive elements in deep-sea turbidites during shallow burial. *Geochimica et Cosmochimica Acta*, 62(4), 643–656.
- Thomson, J., Wilson, T.R.S., Culkin, F. and Hydes, D.J. (1984) Non-steady state diagenetic record in eastern equatorial Atlantic sediments. *Earth and Planetary Science Letters*, 71, 23–30.
- Trentesaux, A., Recourt, P., Bout-Roumazeilles, V. and Tribouillard, N. (2001) Carbonate grain-size distribution in hemipelagic sediments from a laser particle sizer. *Journal of Sedimentary Research*, 71, 858–862.
- Tribouillard, N., Algeo, T., Lyons, T.W. and Riboulleau, A. (2006) Trace metals as paleoredox and paleoproductivity proxies: an update. *Chemical Geology*, 232, 12–32.

- Tribovillard, N., Algeo, T.J., Baudin, F. and Riboulleau, A. (2012) Analysis of marine environmental conditions based on molybdenum-uranium covariation – applications to Mesozoic paleoceanography. *Chemical Geology*, 324–325, 46–58.
- Tribovillard, N.P. (1989) Sédimentation rythmique dans les Marnes Bleues de l'Aptien-Albien du bassin vocontien (France Sud-Est). In: Cotillon, P. (Ed.) *Les événements de la partie moyenne du Crétacé, Géobios Mémoire Spéciale*, 11, 213–224.
- Tyson, R.V. (2001) Sedimentation rate, dilution, preservation and total organic carbon: some results of a modelling study. *Organic Geochemistry*, 32, 333–339.
- Tyson, R.V. (2005) The “productivity versus preservation” controversy: cause, flaws, and resolution. In: Harris, N.B. (Ed.) *The Deposition of Organic-Carbon-Rich Sediments: Models, Mechanisms and Consequences. Special Publications of SEPM*, Vol. 82, 17–33.
- van Aarssen, B.G.K., Bastow, T.P., Alexander, R. and Kagi, R.I. (1999) Distributions of methylated naphthalenes in crude oils: indicators of maturity, biodegradation and mixing. *Organic Geochemistry*, 30(10), 1213–1227.
- van Breugel, Y., Schouten, S., Tsikos, H., Erba, E., Price, G.D. and Sinninghe Damsté, J.S. (2007) Synchronous negative carbon isotope shifts in marine and terrestrial biomarkers at the onset of the early Aptian oceanic anoxic event 1a: evidence for the release of  $^{13}\text{C}$ -depleted carbon into the atmosphere. *Paleoceanography*, 22, PA1210.
- Von Eynatten, H., Barcelo-Vidal, C. and Pawlowsky-Glahn, V. (2003) Modelling compositional change: the example of chemical weathering of granitoid rocks. *Mathematical Geology*, 35, 231–251.
- Weiss, R.F. (1970) The solubility of nitrogen, oxygen and argon in water and seawater. *Deep-Sea Research*, 17, 721–735.
- Weissert, H. (1981) The environment of deposition of black shales in the early Cretaceous: an ongoing controversy. In: Warme, J.E., Douglas, R.G. and Winterer, E.L. (Eds) *The Deep Sea Drilling Project: a Decade of Progress. Society of Economic Paleontologists and Mineralogists, Special Publication 32*, 547–560.
- Weissert, H. (1990) Siliciclastics in the Early Cretaceous Tethys and North Atlantic oceans: documents of periodic greenhouse climate conditions. *Memorie – Società Geologica Italiana*, 44, 59–69.
- Weissert, H., Lini, A., Föllmi, K.B. and Kuhn, O. (1998) Correlation of Early Cretaceous carbon isotope stratigraphy and platform drowning events. A possible link? *Palaeogeography, Palaeoclimatology, Palaeoecology*, 137, 189–203.
- Weissert, H., McKenzie, J.A. and Channell, J.E.T. (1985) Natural variations in the carbon cycle during the Early Cretaceous. In: Sundquist, E.T. and Broecker, W.S. (Eds.) *The Carbon Cycle and Atmospheric  $\text{CO}_2$ : Natural Variations Archean to Present*. Geophysical Monograph Series 32. Washington, DC: AGU, pp. 531–545.
- Westermann, S., Stein, M., Matera, V., Fiet, N., Fleitmann, D., Adatte, T. et al. (2013) Rapid changes in the redox conditions of the western Tethys Ocean during the early Aptian oceanic anoxic event. *Geochimica et Cosmochimica Acta*, 121, 467–486.
- Westermann, S., Vance, D., Cameron, V., Archer, C. and Robinson, S.A. (2014) Heterogeneous oxygenation states in the Atlantic and Tethys oceans during oceanic anoxic event 2. Earth and Planetary. *Science Letters*, 404, 178–189.
- Ziegler, P.A. (1990) *Geological Atlas of Western and Central Europe*. The Hague: Shell International Petrol. Mij, 239 pp.

**How to cite this article:** Caillaud A, Quijada M, Huet B, et al. Turbidite-induced re-oxygenation episodes of the sediment-water interface in a diverticulum of the Tethys Ocean during the Oceanic Anoxic Event 1a: The French Vocontian Basin. *Depositional Rec.* 2020;6:352–382. <https://doi.org/10.1002/dep2.102>